https://doi.org/10.5194/egusphere-2026-4305
Preprint. Discussion started: 4 September 2026
© Author(s) 2026. CC BY 4.0 License.

Operational Earth system hydrology at ECMWF

Cinzia Mazzetti[1], Hannah Cloke[1,2], Dai Yamazaki[3], Gianpaolo Balsamo[1], Souhail Boussetta[1], Jasper Denissen[4], Michel Wortmann[1], Gabriele Arduini[1], Gurpreet Dass[1], Joe McNorton[1], Anna Agusti-Panareda[1], Maliko Tanguy[1], Ervin Zsoter[1], Margarita Choulga[1], Emanuel Dutra[5], Florian Pappenberger[1], Christoph Rüdiger[6], Christel Prudhomme[1]

[1]European Centre for Medium-Range Weather Forecasts, Reading, RG2 9AX, United Kingdom
[2]Department of Meteorology, University of Reading, Reading, RG6 6BB, United Kingdom
[3]Institute of Industrial Science, The University of Tokyo, Tokyo, 153-8505, Japan
[4]Department of Remote Sensing, Helmholtz Centre for Environmental Research (UFZ), Leipzig, 04318, Germany
[5]Instituto Português do Mar e da Atmosfera (IPMA), Lisboa, 1749-077, Portugal
[6]European Centre for Medium-Range Weather Forecasts, Bonn, 53175, Germany

Correspondence to: Cinzia Mazzetti (cinzia.mazzetti@ecmwf.int)

Abstract. The representation of river routing and floodplain dynamics remains a key limitation in many global Earth system and numerical weather prediction models, despite their importance for hydrological extremes, water resources, and land–atmosphere interactions. This paper presents the implementation of a global hydrodynamic river routing capability within the European Centre for Medium-Range Weather Forecasts (ECMWF) Integrated Forecasting System (IFS) through the integration of the Catchment-based Macro-scale Floodplain (CaMa-Flood) model into the ecLand land surface scheme.

The resulting system enables routine simulation of river discharge, water level, and flood inundation extent within a physically consistent Earth system modelling framework. We describe the scientific design and technical developments required to transition from research to operational implementation, including coupling strategies, state initialisation, parallelisation using a basin-based hybrid approach, and integration within ECMWF's research-to-operations workflow. The implementation maintains consistency across multiple configurations ranging from offline experiments to fully coupled forecasts, while meeting operational requirements such as computational efficiency and forecast stability.

The added value of the integrated system is demonstrated through a range of applications, including global water resources monitoring contributing to the World Meteorological Organisation State of Global Water Resources report, real-time ensemble flood forecasting, high-resolution regional simulations, and land-surface diagnostics. Results show that river discharge provides a powerful integrative constraint on the land water cycle and helps identify model deficiencies in hydrological processes. The system also enables the generation of continuous, global, high-frequency hydrological datasets suitable for both operational applications and emerging data-driven modelling approaches.

This work establishes a new capability for global hydrological prediction within an operational Earth system model and provides a framework for future developments toward fully coupled atmosphere–land–river interactions.

https://doi.org/10.5194/egusphere-2026-4305
Preprint. Discussion started: 4 September 2026
© Author(s) 2026. CC BY 4.0 License.

1 Introduction

Earth system models (ESM) represent the Earth's natural processes as a whole, including interactions between the atmosphere, oceans, and land, providing an insight into the complex drivers of high-impact weather and climate, and allowing predictions of the future state of the Earth system (Harrigan et al., 2023). Accurately modelling the interactions between the components of the Earth system improves weather forecasts across different timescales, which is explicitly supported by the World Meteorological Organisation (WMO; World Meteorological Organization, 2019) and widely adopted operationally at global weather forecasting, climate and environmental prediction centres around the world (Bush et al., 2023; ECMWF, 2021; Zhu et al., 2023). Earth system models are also considered vital tools in providing early warnings of upcoming extreme events (Emerton et al., 2018) and provide the basis for "Early warnings for all" (World Meteorological Organization, 2022) with the potential to save lives and reduce economic losses from climate-related disasters (Gettelman et al., 2022).

Many climate-related disasters are directly associated with the lack (e.g., droughts) or excess (e.g., floods) of water across the land surface. The Earth system modelling approach has many advantages for modelling the water cycle: it enables a physically consistent representation of the global water budget, including the distribution and storage of water in rivers, soils, snowpacks, and the atmosphere. The comprehensive and physically consistent treatment of the water cycle supports an accurate simulation of land surface energy exchanges with the atmosphere that regulate surface weather processes and a realistic representation of freshwater fluxes from rivers to the ocean and to the atmosphere through evaporative processes. Together, these components improve atmospheric predictions, which in turn feedback information to strengthen the simulation of the water cycle itself (Harrigan et al., 2020). The accurate representation of runoff generation and river flow within Earth system models is particularly critical for early warning systems (EWS), as it underpins forecasts of floods and droughts, among the most damaging natural hazards worldwide (Jonkman et al., 2024). Hydrological forecasts may be produced directly by ESMs or through post-processing using dedicated hydrological and hydraulic models and tools (Alfieri et al., 2013; Emerton et al., 2016; Harrigan et al., 2020; Pappenberger et al., 2010; Woldemeskel et al., 2025). As early warning systems increasingly incorporate machine-learning and hybrid approaches, the availability of physically and spatially consistent hydrological datasets generated within an Earth system modelling framework becomes essential, as its data serves as the foundation for model training and evaluation. Indeed, Earth system models provide the only modelling environment that ensures the coupled dynamics and physical consistency required to coherently represent land water variables such as soil moisture, runoff, and river discharge. This consistency is increasingly important for emerging machine-learning and emulator approaches, including European Centre for Medium-Range Weather Forecasts (ECMWF) artificial intelligence forecasting system (AIFS; Moldovan et al., 2025; Lang et al., 2024, 2026) and the Earth system components of the Destination Earth programme (DestinE; ECMWF, 2026b), which incorporate elements of the terrestrial water cycle (e.g., runoff) and aim toward fully coupled, data-driven Earth system models. It is also essential for weather

https://doi.org/10.5194/egusphere-2026-4305
Preprint. Discussion started: 4 September 2026
© Author(s) 2026. CC BY 4.0 License.

forecast diagnostics. In this context, river discharge provides a valuable integrative diagnostic of the land water cycle as represented by Earth system models (Prudhomme et al., 2024).

At ECMWF, improving the representation of hydrology and flooding as part of an Earth system modelling approach is a strategic priority (ECMWF, 2025). Large-scale hydrological prediction services must be sustainable across scientific, technical, and computational dimensions (WMO, 2023). Weather forecasting centres are well placed to provide state-of-the-art Earth system data and data assimilation systems, high-performance computing and cloud-based operational environments, the capability to deliver reliable 24/7 forecasts, and the infrastructure and expertise to rapidly adopt emerging developments such as artificial intelligence and machine learning at scale (Harrigan et al., 2023).

The ECMWF land surface scheme, ecLand (Boussetta et al., 2021), is a core component of the Earth system modelling framework underpinning the Integrated Forecasting System (IFS) that provides forecasts across timescales and reanalysis products (Baatz et al., 2021; Prudhomme et al., 2024; Herbert et al., 2024). Although several key hydrological improvements to ecLand were initially explored by Boussetta et al. (2021), many further scientific and technical steps are needed to move from experimental research to operational implementation in an Earth system forecasting model, including operational suite configuration, code parallelisation and optimisation, and cycle testing to ensure that the new developments do not negatively impact the forecast and that they meet the configuration flexibility criteria. Such steps are rarely documented in a comprehensive way, and here we set a benchmark for open documentation of this transition from research to operations.

This paper presents the implementation of a global hydrodynamic river routing capability within ECMWF's Integrated Forecasting System (IFS) through the integration of the Catchment-based Macro-scale Floodplain (CaMa-Flood) into the ecLand land surface scheme. We document the scientific design, technical integration, and operational deployment of this system, including coupling strategies, parallelisation, and verification within the ECMWF research-to-operations (R2O) framework. The resulting system enables, for the first time, routine global forecasts of river discharge, flood stage, and inundation extent within an operational Earth system prediction environment.

2 ECMWF Earth system forecasting approach

2.1 The Integrated Forecast System model components

The Integrated Forecast System (IFS; ECMWF, 2024d; Roberts et al., 2018) is a global Numerical Weather Prediction (NWP) system primarily developed by the European Centre for Medium-Range Weather Forecast (ECMWF), with contributions from partners (including Météo France). It follows an Earth system modelling approach and consists of three components representing physical processes governing the exchange of water, carbon, and energy across the Earth system.

Atmosphere: The atmospheric component simulates the dynamic evolution of atmospheric conditions and their interactions with the land surface and ocean. It represents key processes such as radiation and temperature, cloud microphysics, precipitation, aerosols and greenhouse gases, and includes sub-grid scale processes parameterised within the model framework (ECMWF, 2024b).

https://doi.org/10.5194/egusphere-2026-4305
Preprint. Discussion started: 4 September 2026
© Author(s) 2026. CC BY 4.0 License.

Ocean: The ocean component captures ocean–atmosphere interactions, including the influence of sea-surface roughness on near-surface winds, as well as sea-surface temperature and sea-ice coverage. It integrates multiple specialised models, including ecWAM for waves, NEMO for ocean circulation, and LIM2 for sea-ice processes (e.g., Bidlot and Janssen, 2024).

Land: The land component represents exchanges of water, energy, and carbon at the Earth's surface, enabling realistic simulations of fluxes such as evaporation, runoff, and infiltration across soils, vegetation, snow, and open water bodies. This component is implemented through the ecLand land surface modelling system (Boussetta et al., 2021).

The numerical systems of the atmosphere, ocean and land are solved based on two concepts: the dynamical core and the physical parameterisation. The dynamical core solves the fundamental fluid dynamics equations in the IFS, which are hydrostatic, two-time-level, semi-implicit, and semi-Lagrangian. The physical parameterisation represents the effects of sub-grid scale processes that the dynamical core cannot explicitly resolve due to limitations in computational power and resolution, such as, for example, land-surface processes, radiation, turbulent mixing and cloud microphysics. The physical parameterisations interact with the dynamical core by providing "source terms", influencing the atmospheric motions. Spectral transforms are used to switch between grid-point space, where the physical parameterisations are applied, and spectral space (Wedi et al., 2013, 2020).

2.1.1 Grid and resolution

The IFS employs a reduced Gaussian octahedral grid (Malardel et al., 2016), which allows for a computationally efficient increase in horizontal resolution while ensuring globally uniform grid spacing. Since Cycle 48r1 (June 2023), the IFS has been run at ~9 km horizontal resolution (TCo1279; octahedral reduced Gaussian grid with the spectral truncation number of 1279) for the medium-range and ~36 km horizontal resolution (TCo319) for the sub-seasonal and seasonal ranges. Both systems have 137 vertical levels in the atmosphere. The wave (i.e., ecWAM) and land surface (i.e., ecLand) models operate at the same horizontal resolution as the atmosphere.

2.1.2 Data assimilation and initial conditions

The IFS initial conditions are derived from a data assimilation system that combines recent observations with model simulations to best estimate the state of the Earth system at the time of the forecast. The adjusted states define the initial conditions of the new forecast, drawing from a wide range of in situ and remotely sensed observations. There is a dedicated assimilation system for each of the IFS components: the atmosphere, ocean, ocean waves, land surface and sea ice, all designed to preserve physical consistency across all components (De Rosnay et al., 2022).

2.1.3 Ensemble forecasting

To capture forecast uncertainty, the IFS employs an ensemble forecasting approach with a control forecast and perturbed members based on stochastic, physics-based perturbation techniques (SPP; Lang et al., 2021). This method aims to simulate the likely evolution of the atmosphere and other Earth system components, explicitly accounting for their uncertainty. The

© Author(s) 2026. CC BY 4.0 License.

ensemble size depends on the forecast horizon, comprising 50 members for the medium range (15 days) and 100 members for the sub-seasonal (46 days) or seasonal (7 months) ranges. The Ensemble Data Assimilation (EDA; Isaksen et al., 2010) provides the initial conditions for the ensemble forecast, reflecting uncertainties in observation, boundary conditions and model physics (ECMWF, 2024a).

2.2 The IFS operational configuration

The IFS was developed as a unified software system capable of reliably tracking model changes. The many functions of the IFS are organised within a single high-level programme structure. All model configurations are based on a common top-level calling tree, representing the hierarchical structure of subroutine calls. During execution, the configuration parameters control which routines are activated, thereby defining the specific model configuration and computational workflow (ECMWF, 2024c).

2.2.1 Computational execution

Computational efficiency in the IFS relies on a parallelised implementation designed for high-performance computing architecture based on distributed memory and MPI (Message Passing Interface) message passing. At each timestep, the model executes two main computational blocks: grid-point calculations (physical parameterisation) and spectral calculations (dynamical core) (see Sect. 2.1). Grid-point calculations involve only vertical dependencies, allowing atmospheric columns to be treated independently and distributed flexibly across processors using domain decomposition strategies that optimise load balancing across tasks (e.g., by latitude, zonal wave number, or vertical level). Spectral computations use domain decompositions tailored to the requirements of Fourier and Legendre transforms, with data exchange managed through MPI-based communication (ECMWF, 2024c).

2.2.2 Operational scheduler

The IFS runs are governed by an in-house workflow management software called ecFlow (Bahra et al., 2021), an open-source, modular, and object-oriented Python package designed for running and monitoring complex suites of jobs across a range of machines. A graphical user interface, called ExpERT (Experiment Edit and Run Tool, formerly known as PrepIFS; Burton et al., 2025), replicates the scientific components of the IFS and allows for easy interaction with the IFS calling tree to create, configure and submit IFS experiments. ExpERT is available to the IFS developers and ECMWF Member and Co-operating States' scientists.

2.2.3 Meteorological Archival and Retrieval System (MARS)

At ECMWF, outputs from operational systems (e.g., IFS, ERA5, SEAS5) and research experiments are archived in the Meteorological Archival and Retrieval System (MARS), which stores gridded data using the WMO General Regularly-distributed Information in Binary standard format (GRIB, edition 2 used in operation from 2026). MARS provides a single,

https://doi.org/10.5194/egusphere-2026-4305
Preprint. Discussion started: 4 September 2026
© Author(s) 2026. CC BY 4.0 License.

unified repository, enabling consistent archival and retrieval workflows across variables and experiment types, therefore enhancing efficiency and reproducibility.
Archiving in MARS requires each variable to be defined in the WMO catalogue (https://wmo.int/latest-version, last access: 24 March 2026) and assigned a unique GRIB2 parameter identifier code linked to its metadata (e.g., variable description, time dimension, and unit). New variables can only be added following WMO approval. As of January 2026, MARS includes 7397 distinct GRIB2 parameter definitions, accessible via the ECMWF Parameter Database online tool at: https://codes.ecmwf.int/grib/param-db/ (last access: 24 March 2026).

2.3 Implementing changes in the IFS: the research-to-operations workflow

2.3.1 Development workflow

Given the complexity of the IFS, any proposed modification, whether related to physical parametrisation, new processes or prognostic variables, computational performance or code maintenance, must undergo a structured evaluation process before being added to the operational production. Model upgrades are introduced regularly, through clearly defined releases ("Cycles"), generally once per year, with a version number and associated documentation. At the time of writing, Cycle 49r1 (implemented in November 2024) is operational, while Cycle 50r1 is planned for 2026.
Final acceptance of a cycle for operational production requires the successful completion of an experimental suite (the e-suite), which is designed to test all NWP changes at operational resolution. Performance is assessed against physical consistency, forecast skill metrics, and demonstrated scientific added value compared to the currently operational version (the o-suite). Because e-suites are computationally demanding, they represent the final stage of testing and are preceded by a hierarchical sequence of experiments within the formal research-to-operations (R2O) framework (Buizza et al., 2017).
The progression from research experiments to operational implementation consists of distinct phases of increasing complexity and system integration, designed to ensure robustness and operational readiness.
Alpha testing: This is the first and most comprehensive phase of the ECMWF R2O testing hierarchy and is conducted by research scientists. The Alpha testing provides a structured way to gradually merge separate developments into system versions of increasing completeness, from single experiments to the e-suite, making it easier to identify meteorological interactions and pinpoint the source of technical problems. Throughout this phase, objective evidence is gathered using standardised metrics to determine if a proposed change improves forecast quality or enhances the realism of the simulated Earth system. It also evaluates the impact of changes on computing resources, ensuring they remain affordable and do not delay operational forecast delivery. The Alpha phase is organised in 5 stages (ad hoc testing, testing against controls, thematic merging, incremental builds, and high-resolution e-suite) and it lasts for a minimum of 7 months (Buizza et al., 2017).
Beta testing: In this phase, the new IFS model (the e-suite) runs in parallel with the operational IFS model (the o-suite) for about two months to ensure it is stable in a real-time environment and results match those from the end of the Alpha testing.

https://doi.org/10.5194/egusphere-2026-4305
Preprint. Discussion started: 4 September 2026
© Author(s) 2026. CC BY 4.0 License.

Release candidate testing: This is the phase immediately before the release. The new IFS model (the e-suite) is frozen, meaning no changes altering the model's outputs are allowed. ECMWF users are given final data samples from the new model to ensure their own systems (like those in Member States) are ready for the switch. Depending on the complexity of the new developments and the impact on the users, this phase can last between one and three months.

The progress of the e-suite is closely monitored through the three phases. The final decision to release a cycle candidate is taken after the e-suite has covered a large enough sample of cases, typically at least two full seasons (one summer and one winter) of analyses and forecasts, to ensure the results are statistically significant (Buizza et al., 2018).

An example of the implementation process is provided by Cycle 49r1. The cycle began with a contribution window from January to June 2023, during which scientific developments were submitted for inclusion. The Alpha testing phase started in July 2023 and involved multiple rounds of merging to produce successive system versions. During this phase, unexpected discrepancies between the e-suite and system version v11 were identified at TCo1279 resolution, requiring additional testing and extending the phase by several months. Cycle 49r1 was declared ready for implementation in January 2024, following completion of the e-suite incorporating all system developments. Release candidate testing commenced in August 2024, and Cycle 49r1 was operationally implemented with the 06 UTC run on 12 November 2024. Further details are available at: https://confluence.ecmwf.int/display/FCST/Implementation+of+IFS+Cycle+49r1 (last access: 24 March 2026).

2.3.2 Code standards

The entire IFS code is complex, mainly written in Fortran 90, with some parts also in C, and C++, with a scripting interface and module coupling mainly available as Shell and Python scripts. Developers must adhere to strict coding standards that govern naming conventions, code layout, parallelisation practices, and prohibited actions (see https://sites.ecmwf.int/docs/ifs-arpege-coding-standards/ (last access: 24 March 2026)). The code sharing, maintenance and development are done through the Git infrastructure, allowing flexible maintenance and industry-standard software management practices (Sleigh et al., 2025).

2.3.3 Code availability

The IFS source is not publicly available, accessible only by ECMWF and its Member and Co-operating States (Sleigh et al., 2025). However, parts of the IFS code are open source, and they are available on the ECMWF-IFS GitHub repository under the Apache-2.0 license at: https://github.com/ecmwf-ifs (last access: 24 March 2026).

To promote and facilitate co-development and collaboration, a community-based version of the IFS, distributed under the name OpenIFS (Carver, 2022), is available as open-source software under the Apache-2.0 license at: https://github.com/ecmwf-ifs/openifs (last access: 24 March 2026). The land component of IFS, ecLand 2.0 has also been released as open-source software at: https://github.com/ecmwf-ifs/ecland (last access: 24 March 2026).

2.3.4 Scientific acceptance

Scientific acceptance of IFS developments is assessed through a hierarchy of experiments of varying complexity (see Fig. 1), designed to provide objective evidence that proposed model changes improve forecast skill, enhance physical realism, or deliver valuable new products to ECMWF users. New ecLand land surface developments are subject to the following structured evaluation framework.

1D Site runs: These are single-site offline surface experiments (i.e., 1-way atmosphere-to-land-to-rivers coupling, see Sect. 3.3.1) in which the model is driven by prescribed meteorological forcings without feedback to the atmosphere. Each simulation is performed on a single grid cell corresponding to the coordinates of the observation site. Experiments are conducted across several sites representing a range of environmental conditions (e.g., vegetation types, climate regions, and soil types) and depending on the availability of observational data (e.g., FLUXNET; Pastorello et al., 2020). They are at the base of ECMWF's testing hierarchy and are often used for very early and computationally inexpensive testing to gain initial insights into the meteorological impact of changes to soil, snow, or vegetation before moving to more expensive global configurations.

2D Area/Global runs: These are offline surface experiments (i.e., 1-way atmosphere–to-land-to-rivers coupling, see Sect. 3.3.1) in which specific components of the IFS, such as the land surface or ocean waves, are run in isolation across a two-dimensional grid, regional or global, without being coupled to the full three-dimensional atmospheric model and using prescribed atmospheric forcing, similar to the ERA5-Land (Muñoz-Sabater et al., 2021) configuration. They ensure that new scientific developments remain stable and realistic across the global or regional geography of the Earth system before progressing to high-resolution research experiments.

3D Coupled GCM and GCM+DA runs: These are coupled Global Circulation Model (GCM) experiments, with or without Data Assimilation (DA) (i.e., 2-way atmosphere-land and 1-way land-to-rivers coupling, see Sect. 3.3.1) where the three-dimensional atmospheric model is dynamically linked to other Earth system components. In 3D coupled runs, two-way interactions between the atmosphere, the land surface and the ocean significantly increase the complexity and realism of the simulations, allowing for the evaluation of the impact of the new developments on NWP scores (with or without data assimilation).

Depending on the variable of interest (e.g., surface state variables and fluxes, river discharge, CO_2 concentration and global budget), different verification toolboxes are used to compute scientific performance metrics (see Fig. 1). Surface state variables and fluxes, for example, are evaluated with an ECMWF internal toolbox (LANDVER), which provides independent validation of soil moisture and soil temperature against in situ observations from the International Soil Moisture Network (ISMN; Dorigo et al., 2021) and FLUXNET (Pastorello et al., 2020). For operational evaluation, reanalysis products and SYNOP observations are used within ECMWF's integrated verification toolbox (IVER) and ECMWF's quality assessment and verification system (QUAVER). IVER is designed for verification against analysis, while QUAVER generates summary "scorecards" that provide a rapid overview of differences in forecast skill between model configurations

https://doi.org/10.5194/egusphere-2026-4305
Preprint. Discussion started: 4 September 2026
© Author(s) 2026. CC BY 4.0 License.

(see Fig. 2), including verification against analysis and SYNOP observations. Together, these tools enable a comprehensive intercomparison of NWP experiments, including forecast skill metrics, changes in analysis and model climatology, and computational performance.

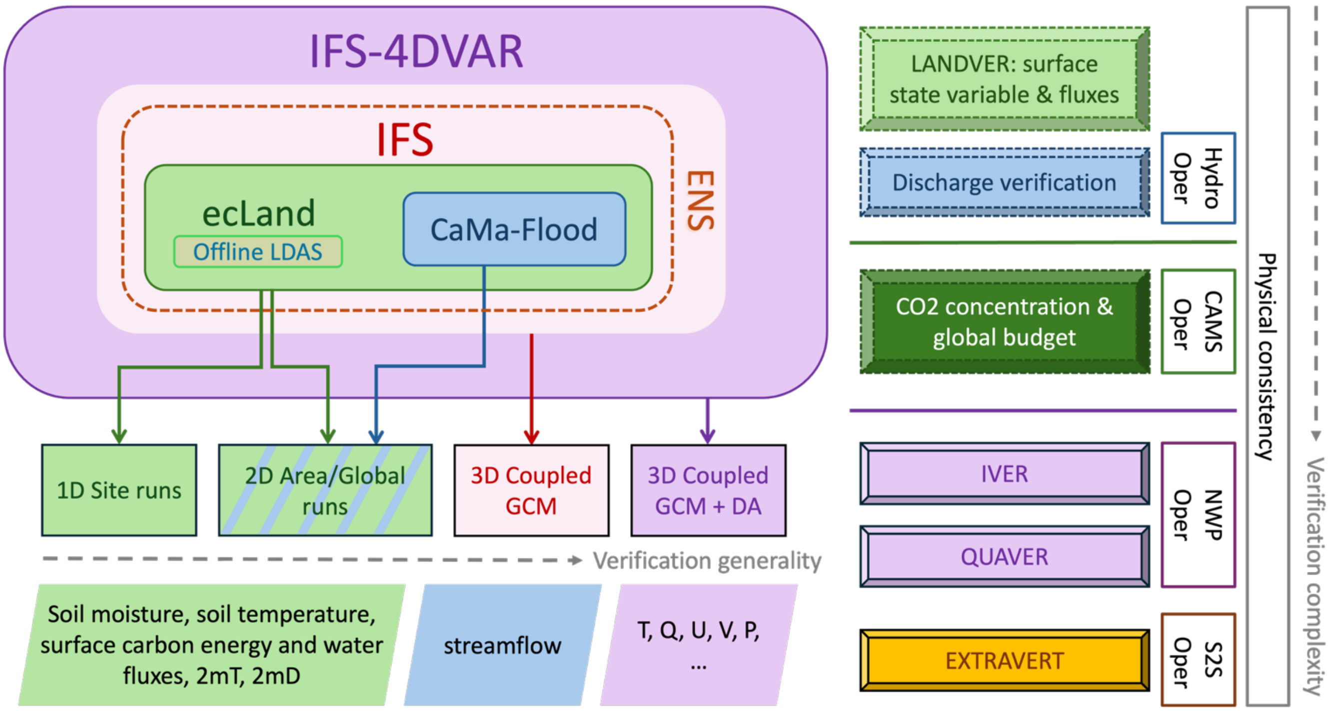

Figure 1: Schematic of the different experiment configurations used for the IFS scientific acceptance for different variables (left) and associated verification toolboxes (right). The colours indicate the different components of interest (atmosphere: purple, land: green, carbon: dark green, rivers: blue, orange: all).

QUAVER provides the core operational verification diagnostics at ECMWF, generating statistics, plots, and summary scorecards (see Fig. 2). These scorecards typically synthesise performance differences between a new experimental cycle (e-suite) and the current operational version (o-suite). Their primary purpose is to provide objective evidence supporting the decision on whether a new IFS cycle is ready for operational implementation. They allow for the rapid identification of statistically significant improvements or degradations across atmospheric variables, geographical regions, and forecast lead times (Buizza et al., 2017).

Verification includes comparisons against both the experiment's own analysis and independent observations, covering upper-air and near-surface variables (e.g., geopotential height, wind speed, and temperature) aggregated over large geographical domains (the Northern and Southern Hemispheres, the tropics, and Europe). Standard metrics include biases, root mean square error (RMSE), correlation, continuous ranked probability score (CRPS) and ensemble spread alongside statistical significance. In addition, 'headline scores' are calculated to monitor long-term trends in forecast performance and quantities representative of the evolution of large-scale flow or high-impact weather (see for more detail

https://doi.org/10.5194/egusphere-2026-4305
Preprint. Discussion started: 4 September 2026
© Author(s) 2026. CC BY 4.0 License.

https://www.ecmwf.int/en/forecasts/quality-our-forecasts, last access: 24 March 2026, and https://confluence.ecmwf.int/display/FUG/Section+6.2.1+ECMWF+headline+scores, last access: 24 March 2026).

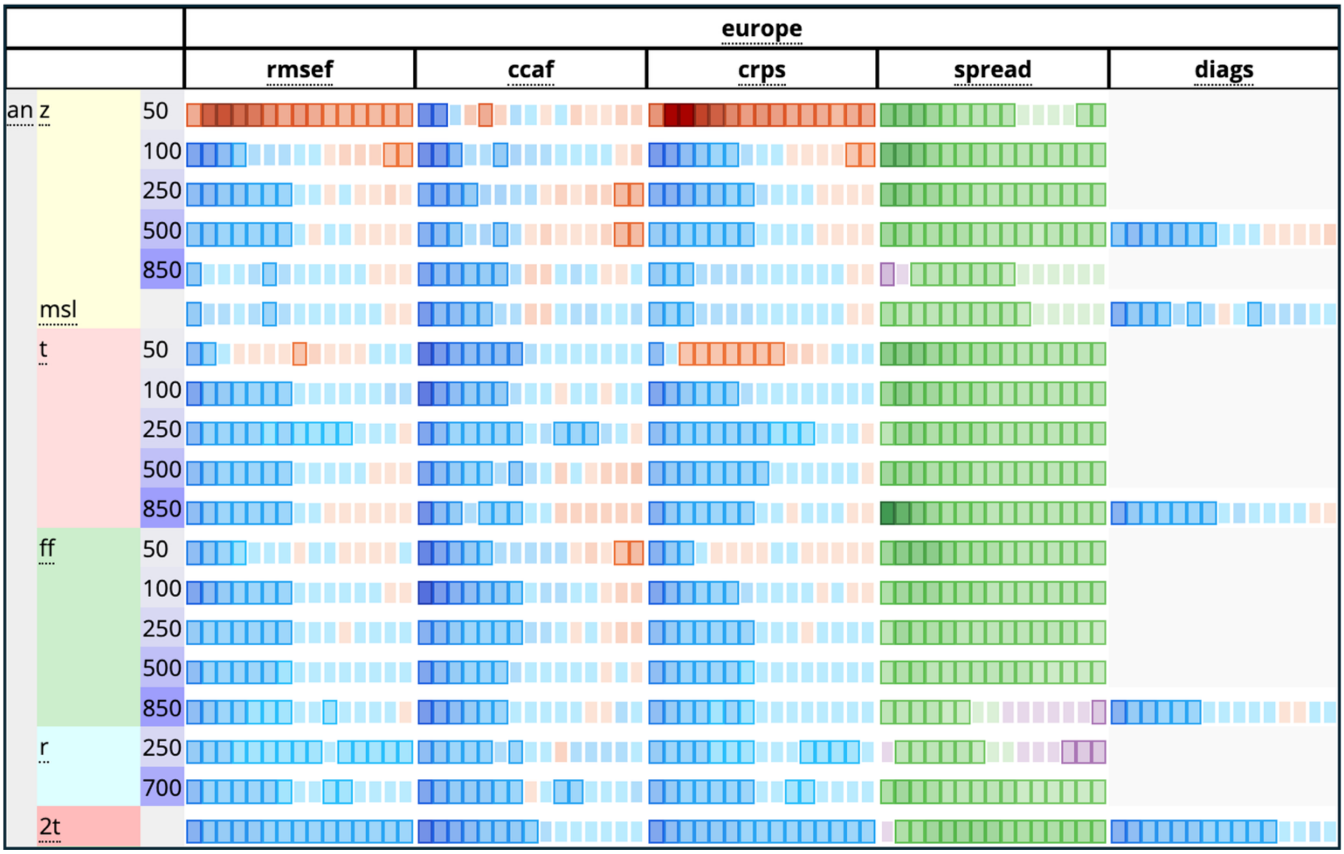

Figure 2: Extract of Cycle 49r1 ENS scorecard for Europe. Score metrics (columns; rmsef = root mean square error of ensemble mean, ccaf = anomaly correlation of ensemble mean, crps = continuous ranked probability score, spread = ensemble spread, diags = diagonal score) for given variables and lead times (rows; z = geopotential height, msl = mean sea level pressure, t = temperature, ff = wind speed, r = relative humidity, 2t = 2 m temperature) against analysis (an), shown as colour-coding (red = the experiment (e-suite) is worse than the control, blue = the experiment (e-suite) is better than the control, purple = the experiment (e-suite) is more active than the control, green = the experiment (e-suite) is less active than the control). Colour hue and saturation are proportional to the normalised difference value. A colour-framed cell indicates the differences are statistically significant on 95% confidence level. Where the differences are not significant on at least 50% level, they are masked by a light grey box (option 50%/95%). Source: https://sites.ecmwf.int/ifs/scorecards/ (last access: 24 March 2026).

2.3.5 Computational performance

A technical evaluation is conducted on computational cost, memory usage and code refactoring requirements to ensure that model upgrades remain affordable and do not delay forecast delivery, especially when changes impact the horizontal/vertical resolution and timesteps of different configurations. If a scientific change negatively impacts computational performance, developers are generally expected to find ways to make the change cost-neutral, using technical solutions like code parallelisation and reducing variable precision.

3 Integrating rivers into the IFS

3.1 IFS land surface system: ecLand

The ecLand modular framework (Boussetta et al., 2021; ECMWF, 2024b) represents the land component of the IFS. It is a physically based modelling system that describes the movement of energy, water, and carbon into the soil column and the exchange of fluxes (energy, water, momentum, and carbon) with the atmosphere. The surface-atmosphere interface employs a tile scheme with eight land cover types (e.g., broadleaf forest, cropland, and grassland) and two water surface types to represent sub-grid heterogeneity. The model has evolved to include many physical sub-modules that represent the main features of the water, energy and carbon cycles, including, for example, soil hydrology processes (Balsamo et al., 2009), snow (Dutra et al., 2010; Arduini et al., 2019), lakes (Balsamo et al., 2012), vegetation representation (Boussetta et al., 2013a), land-atmosphere carbon exchanges (Boussetta et al., 2013b), coupling with ocean (Balsamo et al., 2017), urban parametrisation (McNorton et al., 2021), glaciers and ice sheets (Arduini et al., 2026). The ecLand framework can exchange land feedback with the IFS atmospheric component (i.e., 2-way atmosphere-land coupling; see Sect. 3.3.1), or it can run in an offline coupling configuration, using external atmospheric variables as forcings at the interface and without accounting for any feedback to the atmosphere (i.e., 1-way atmosphere-to-land coupling; see Sect. 3.3.1). The offline configuration can run at scales from a single point/grid to global, with a single grid runtime of under one minute, allowing a quick cycle of developing, compiling, running and debugging new developments as detailed in the scientific acceptance section (see Sect. 2.3.4).

To enable external contributions and to support new developments, including hydrological components, ecLand 2.0 has been released as open-source software on the ECMWF-IFS GitHub repository under the Apache-2.0 license at: https://github.com/ecmwf-ifs/ecland (last access: 24 March 2026).

3.2 Global-scale distributed river model: CaMa-Flood (Catchment-based Macro-scale Floodplain)

The river routing component of ecLand is the Catchment-based Macro-scale Floodplain model (CaMa-Flood). CaMa-Flood is a hydrodynamic model that can route surface and subsurface runoff through a river network and translate that volume of water into river discharge, water level and inundation extent. CaMa-Flood was developed for large-scale (continental to global) river flow simulations (Yamazaki et al., 2011, 2013; Yamazaki, 2025), targeting multiple applications such as flood risk assessment (Hirabayashi et al., 2021), real-time flood forecasting (Ma et al., 2021), and coupling with Earth system models (Nitta et al., 2020). A river network is discretised into unit catchments that approximately correspond to driving data grid cells, such as runoff from a hydrological model on a regular geodetic grid. All time-invariant parameters for the unit catchments are derived from high-resolution sources, mainly a digital elevation model (DEM) and a digital hydrography map that provide information on river gradient, bank elevation and floodplain hypsometry. Each unit catchment represents a river reach and its floodplain, with river discharge and water stages simulated without the need for high-resolution 2D simulations. Within ecLand, the CaMa-Flood component is regularly updated to incorporate all relevant external

https://doi.org/10.5194/egusphere-2026-4305
Preprint. Discussion started: 4 September 2026
© Author(s) 2026. CC BY 4.0 License.

developments, such as the reservoir operation scheme (Hanazaki et al., 2022) and the simple flood protection representation (Zhao et al., 2025).

The model code is implemented in Fortran and is available as open-source software under the Apache-2.0 license at: https://github.com/global-hydrodynamics/CaMa-Flood_v4 (last access: 24 March 2026).

3.3 Coupling IFS and CaMa-Flood

Integrating river routing within IFS introduces some coupling complexity, with rivers exchanging water with the rest of the land surface scheme and, in experimental configurations still under development, also directly or indirectly with the atmosphere. At the same time, coupling strategies must remain sufficiently flexible to support both operational forecasting and research experimentation, with research applications typically demanding substantially greater configurability with the ability to adjust coupling frequencies, test alternative process representations and different data exchange pathways (Kousal et al., 2026).

Besides data exchange, river initial conditions (i.e., river variables' state at the first timestep of a simulation) must be managed correctly in different contexts, such as operational forecasts, diagnostic and research experiments. The river discharge and water storage states (e.g., riverbed and floodplain discharge, river depth, riverbed and floodplain storage and, when activated, groundwater storage and bifurcation channel discharge) need to be available at the beginning of all computation timesteps. CaMa-Flood reads the information from state files, either produced by a previous simulation (warm start) or empty storage values (cold start). When running with a cold start, a spin-up period is needed before the model can deliver a coherent physical representation of the river flow, and the results of this spin-up should be disregarded (Santos et al., 2019).

Code-wise, a key requirement of the IFS and CaMa-Flood integration was the ability to maintain the same code base across all configurations, spanning operational forecasting, research experimentation, and diagnostic applications to support rapid development cycles (see Sect. 3.1) while facilitating a seamless research-to-operations transition.

Finally, regarding the impact of CaMa-Flood computation time on IFS, CaMa-Flood was originally developed for global-scale applications and has a substantially lower computational cost than land surface models (Nitta et al., 2020). However, its original OpenMP-based parallelization was insufficient to support kilometre-resolution operational global weather and hydrological forecasting within the IFS, and refactoring was therefore required.

The integration of CaMa-Flood within IFS introduces multiple levels of coupling complexity. In its current operational configuration, the system supports a one-way coupling from land to rivers, where runoff generated by ecLand is routed through the river network without feedback to the land surface or atmosphere. Experimental configurations extend this framework to fully coupled systems, enabling feedback through evaporation from inundated areas and interactions with soil moisture. These configurations provide a flexible framework for both operational forecasting and process-oriented research.

https://doi.org/10.5194/egusphere-2026-4305
Preprint. Discussion started: 4 September 2026
© Author(s) 2026. CC BY 4.0 License.

3.3.1 Information exchange

Three atmosphere-land-river coupling configurations were designed and implemented to meet all modelling requirements (see Fig. 3).

Operational configuration: The operational forecast system as of January 2026 uses a 2-way atmosphere-land exchange with feedback between land and atmosphere (e.g., evapotranspiration), while land-to-rivers exchange remains 1-way with no river feedback to either land or atmosphere (see Fig. 3a). Rivers receive surface and subsurface runoff from the land surface model at each internal coupling timestep, with a coupling frequency equal to the land surface scheme timestep (default: 1 hour). Runoff is routed to the river channel through two pathways: direct routing (overland flow) uses surface runoff only, while subsurface runoff first percolates through the land's soil column vertically and then enters a groundwater reservoir that delays release to the river channel using a linear reservoir with a specified time scale. For lakes that are explicitly represented in ecLand (i.e., 'resolved lakes', Balsamo et al., 2012), the total runoff is set equal to the total precipitation. A mass-conservative re-gridding module handles the interface between the land's reduced Gaussian octahedral grid and the rivers' geographic grid.

2-way coupled configuration: This experimental configuration implements a bidirectional atmosphere-land-rivers exchange, with information on the flooded fraction sent from rivers to land and treated as an inland open-water body, evaporating to the atmosphere. Simultaneously, the evaporation withdraws water from the river system storage, providing feedback to the rivers discharge and flooded area (see Fig. 3b). This implementation also allows for future evolutions, like incorporating additional river-to-land feedback mechanisms through infiltration of the flooded water.

1-way coupled configurations: In these unidirectional configurations, information propagates sequentially from atmosphere to land to rivers (see Fig. 3c). The absence of feedback mechanisms permits a flexible combination of different model components and data sources as building blocks of the modelling chains, thereby enabling exploration of diverse research questions, model intercomparisons, and diagnostic analyses at less computational cost. The atmospheric component provides meteorological forcing (e.g., IFS, AIFS, ERA5, gridded observations, DestinE), while the land component functions as the rainfall-runoff transformation module (e.g., ecLand). The 1-way coupled configurations are indispensable for research and diagnostic applications by allowing the river routing component to be forced with runoff and precipitation inputs of arbitrary time and horizontal spatial resolutions from any independent land surface scheme or experiment, regardless of whether the source is a physics-based or data-driven model. The coupling frequency between land and rivers is configurable from hourly to daily intervals, with runoff being time-averaged over the coupling interval when produced at a higher temporal frequency. Direct routing to river channels (overland flow) can be configured to receive either total runoff (the sum of surface and subsurface components) or surface runoff exclusively. In the latter case, subsurface runoff is directed to a groundwater reservoir that delays water release to the river channel according to a linear reservoir time scale, representing groundwater flow processes.

https://doi.org/10.5194/egusphere-2026-4305
Preprint. Discussion started: 4 September 2026
© Author(s) 2026. CC BY 4.0 License.

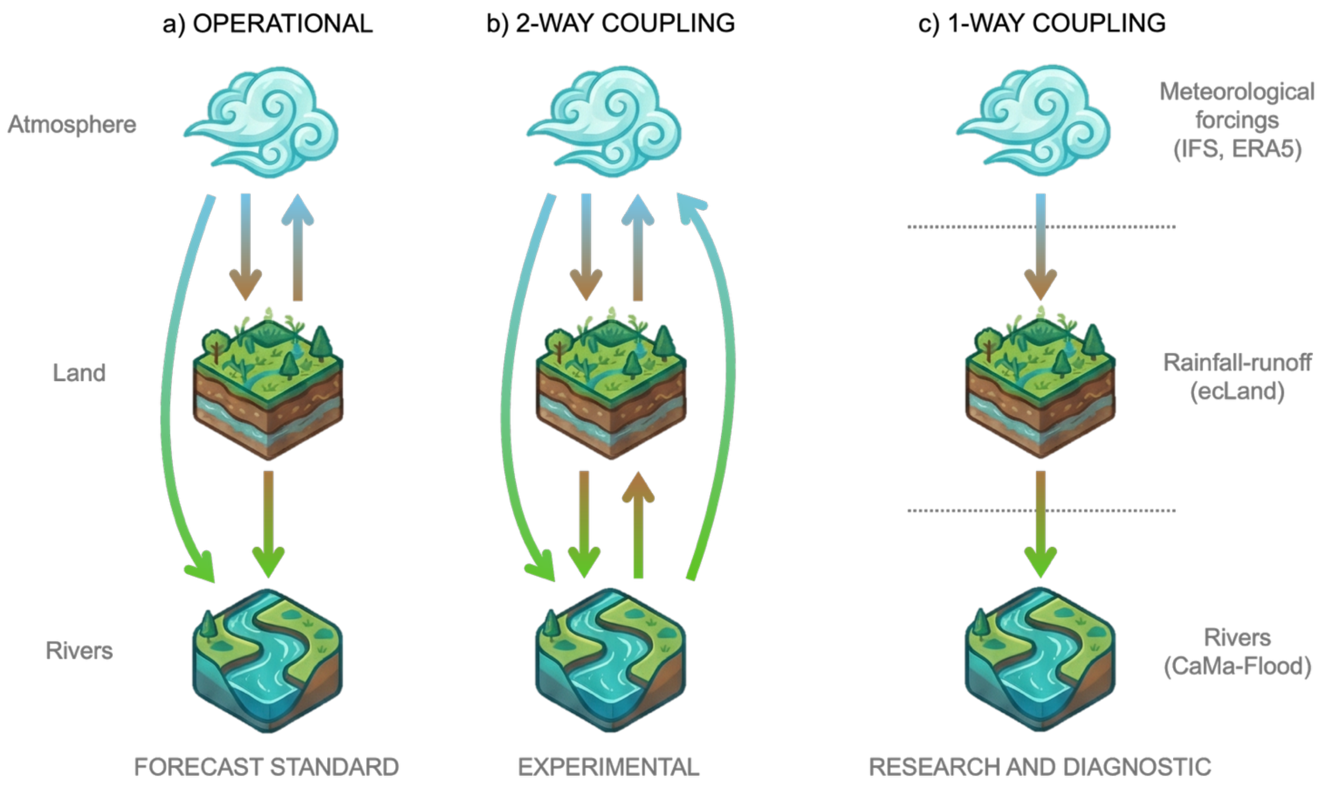

Figure 3: Schematic representation of coupling configurations in the IFS. (a) Operational configuration (January 2026): 2-way atmosphere-land coupling with 1-way land-to-rivers transfer of surface and subsurface runoff. Used for IFS operational forecasts. (b) 2-way coupling configuration: bidirectional feedback across all components, still in experimental development. (c) 1-way coupling configurations: unidirectional flow from atmosphere to land to rivers, enabling independent selection of forcing, rainfall-runoff, and routing components for diagnostic and research applications. Arrows indicate the data exchange direction. The dashed arrow represents the optional input from the atmosphere when the 1-way coupling configuration runs with the land and river components only, using only runoff as input to the rivers.

For example, a 1-way coupled configuration (see Fig. 3c) can be used for reanalysis-driven simulations using ERA5 forcings and a 1-way atmosphere-to-land-to-rivers coupling to regenerate ERA5 land (Muñoz-Sabater et al., 2021) variables by running the latest land physics version from IFS while still using ERA5 atmospheric variables as forcings.

Additionally, the flexible control of the internal data exchange frequency in the different configurations allows running quick experiments, testing and evaluating advances in areas such as the Land Data Assimilation System (Fairbairn et al., 2019; Herbert et al., 2024) or 2-way atmosphere-land-rivers coupling.

3.3.2 Initialisation

Initial conditions handling was implemented to support the different coupling configurations, with dedicated restart strategies depending on the configuration and experiment type. For short-range forecasts, warm starts are performed using only river channel and floodplain storage state files. In contrast, multi-year simulations (e.g., reanalysis) require the full set

© Author(s) 2026. CC BY 4.0 License.

of model state files to ensure bit-identical restarts. To shorten the simulations' spin-up period, the capability to use seasonal averages obtained from climatological runs at different rivers' spatial resolutions was added to the cold start.

3.3.3 Software flexibility and modularity

The necessary software flexibility and modularity were achieved through the refactoring of the original land surface and CaMa-Flood codes to improve calculation workflows (e.g., initialisation, restart, timestep and data exchange control, and output), modularise physics subroutines and variables, and enable interoperability and flexible coupling (e.g., consistent naming convention). The refactoring of the land surface component introduced the capability to represent parameters associated with parameterised climate processes as spatially uniform values, spatially distributed 2D fields, or hybrid combinations of both, thereby enabling future parameter calibration and optimisation exercises. The refactoring also introduced a flexible I/O scheme supporting both binary and NetCDF outputs and ensured alignment with ECMWF coding standards. The CaMa-Flood output was extended to enable direct GRIB2 output (via ECMWF's output abstraction library MultIO, Sármány et al., 2024).

3.3.4 Computation efficiency of the river model

A new hybrid MPI/OpenMP parallelization option was introduced in ecLand to enable the use of multiple computational nodes. Because river routing involves horizontal water exchanges between upstream and downstream grid cells, MPI parallelization is more challenging for river models than for vertically one-dimensional land surface models (Mizukami et al., 2021). To minimize inter-node communication, grid cells are grouped by river basin and assigned to a single MPI node, within which OpenMP parallelization is applied. This basin-based domain decomposition largely avoids MPI communication during river discharge calculations, except for runoff input distribution, timestep synchronization, and output collection, resulting in improved computational efficiency.

In addition to the hybrid MPI/OpenMP parallelization, a single-precision compilation mode was introduced for variables not required for strict water balance calculations. Variables requiring strict water balance represent only about 2–3% of the total, resulting in a negligible impact on simulation time while nearly doubling computational speed.

3.3.5 Scientific verification

CaMa-Flood integration in IFS adhered to the stages prescribed by the IFS research-to-operations development workflow (see Sect. 2.3), testing both scientific acceptance and computation performance. NWP scientific verification followed the science acceptance tests, where positive or neutral changes to key atmospheric variables are required. We performed the full suite of tests required by the NWP verification framework (e.g., offline experiments, analysis (AN) type and ensemble (ENS) type experiments). Verification experiments quantified differences in core diagnostic variables (e.g., 2 m temperature, soil temperature, volumetric soil water, runoff, skin temperature, and mean sea-level pressure) between baseline and coupled IFS and CaMa-Flood configurations. Bit-identical behaviour of IFS was demonstrated for both 1-way atmosphere-to-land

© Author(s) 2026. CC BY 4.0 License.

and land-to-rivers coupling configurations, confirming that the integration of CaMa-Flood did not introduce unintended perturbations into the atmosphere component.

3.4 Geospatial data

The integration of rivers within the IFS requires a set of geospatial datasets. These include information on river topology, like river channel width, depth, friction, slope and length, and CaMa-Flood modelling information, like unit catchment, outlet elevation, floodplain elevation profile and routing topology, including floodplain bifurcation pathways (Yamazaki et al., 2019). Most datasets are derived from Earth observation products, some rely on simulated information, for example, the river channel depth parameter, which is defined as a power-law function of annual mean river flow, while others adopt default values that can be further tuned, such as riverbed roughness.

All geospatial information is available at 15, 6, 3 and 1 arcminute resolutions. The spatial resolution of rivers can be coupled to any spatial resolution of the land in both the 1-way or 2-way coupling schemes (see Sect. 3.3.1). In the current operational setup, a 3 arcmin river resolution is adopted, providing a balance between computational cost and hydrological realism. This resolution enables a sufficiently detailed representation of river networks and floodplain dynamics while remaining compatible with the runtime constraints of the IFS.

A new river basin discretisation, describing how river basins are connected, was introduced to enable the MPI/OpenMP hybrid parallelisation of the IFS rivers component (see Sect. 3.3.4 on computation efficiency of the river model). The corresponding map was derived by assigning the same MPI node to all river basins connected through bifurcation channels, equalising the number of grid cells allocated to each MPI node to balance the computational load (see Fig. 4). Note that the largest connected river basins (Amazon and Orinoco rivers, St. Lawrence and Mississippi rivers) contain almost 6% of all land grids, and that the maximum MPI nodes available under this parallelisation scheme is 16 when river bifurcations are considered. If a few connecting channels (e.g., the Casiquiare Canal connecting the Amazon and Orinoco rivers) are neglected, the maximum number of MPI nodes can be increased to 30. Neglecting river bifurcations reduces computational cost but introduces systematic approximations in simulated river discharge and water levels downstream of the bifurcation in both the donor and receiving river systems. These discrepancies arise from the mismatch in flowing water volume between the model representation and reality, where, in nature, part of the flow is diverted from one basin to another.

https://doi.org/10.5194/egusphere-2026-4305
Preprint. Discussion started: 4 September 2026
© Author(s) 2026. CC BY 4.0 License.

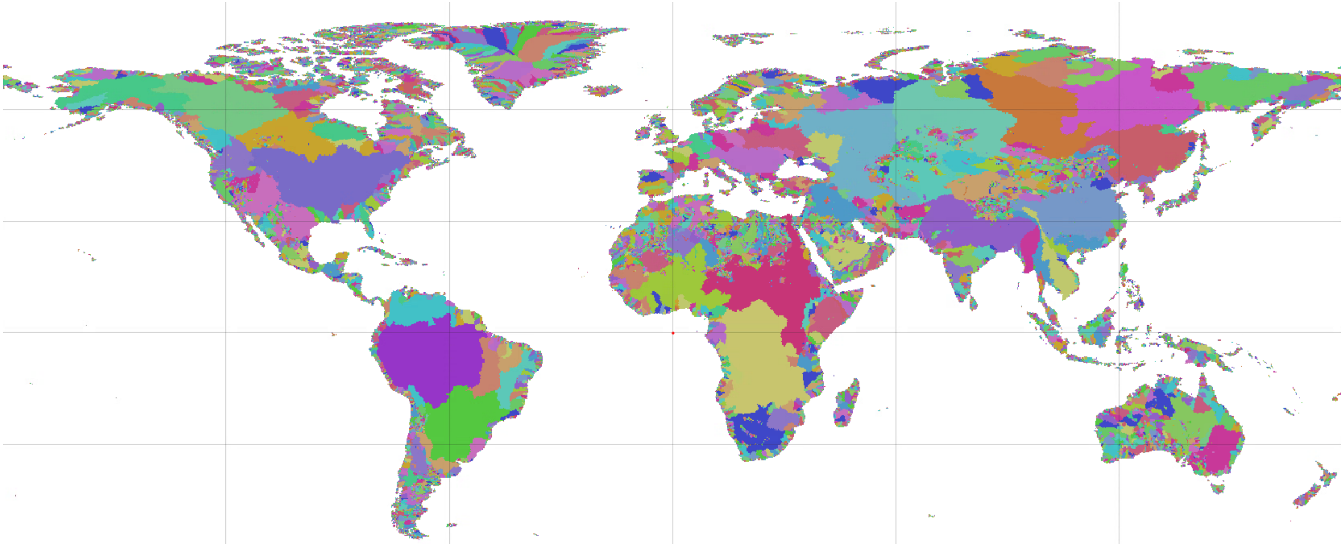

Figure 4: MPI region map for 30 MPI processes at 15 arcminute spatial resolution, with each colour representing the model grid cells belonging to a different MPI process.

3.5 Data output and archival

Integrating rivers in the IFS required the addition of 36 new river flow and storage variable codes (see Table 1), both averaged and instantaneous, in the GRIB2 parameter database, including floodplain discharge, floodplain water storage, and floodplain flooded fraction. The use of the MultIO library (see Sect. 3.3.3 on software flexibility and modularity) enables direct archival of river-related outputs to MARS without requiring additional formatting, transformation, or re-gridding steps.

Table 1: List of CaMa-Flood variables encodable in GRIB2. Variable Short Name and Variable Description refer to the internal name and description used by MARS for the variable, respectively. GRIB2 code describes the variable's code in the parameter database.

Variable Short Name	**Variable Description**	**Unit**	**GRIB2 code**
avg_dis	Time-mean discharge from rivers or streams	$m^3\ s^{-1}$	235270
flddep	Floodplain depth	m	240035
avg_flddep	Time-mean floodplain depth	m	235274
fldffr	Floodplain flooded fraction	Proportion [0 to 1]	240036
avg_fldffr	Time-mean floodplain flooded fraction	Proportion [0 to 1]	235275
fldfar	Floodplain flooded area	m^2	240037
avg_fldfar	Time-mean floodplain flooded area	m^2	235276

https://doi.org/10.5194/egusphere-2026-4305
Preprint. Discussion started: 4 September 2026
© Author(s) 2026. CC BY 4.0 License.

rivfr	River fraction	Proportion [0 to 1]	240038
avg_rivfr	Time-mean river fraction	Proportion [0 to 1]	235277
rivar	River area	m^2	240039
avg_rivar	Time-mean river area	m^2	235278
rivcffr	Fraction of river coverage plus river related flooding	Proportion [0 to 1]	240040
avg_rivcffr	Time-mean fraction of river coverage plus river related flooding	Proportion [0 to 1]	235279
rivcfar	Area of river coverage plus river related flooding	m^2	240041
avg_rivcfar	Time-mean area of river coverage plus river related flooding	m^2	235280
pthflw	Floodpath outflow of water	$m^3 s^{-1}$	240034
avg_pthflw	Time mean floodpath outflow of water	$m^3 s^{-1}$	235403
fldout	Floodplain outflow of water	$m^3 s^{-1}$	240033
avg_fldout	Time mean floodplain outflow of water	$m^3 s^{-1}$	235402
rivout	River outflow of water	$m^3 s^{-1}$	240032
avg_rivout	Time mean river outflow of water	$m^3 s^{-1}$	235401
fldsto	Floodplain storage of water	m^3	240015
avg_fldsto	Time mean floodplain storage of water	m^3	235399
rivdph	River depth	m	240031
avg_rivdph	Time mean river depth	m	235400
rivsto	River storage of water	m^3	240014
avg_rivsto	Time mean river storage of water	m^3	235398
wse	Water surface elevation	m	240042
avg_wse	Time-mean water surface elevation	m	235412
grfr	Groundwater return flow rate	$m^3 s^{-1}$	240043
avg_grfr	Time-mean groundwater return flow rate	$m^3 s^{-1}$	235413
rivfldsto	River and floodplain storage	m^3	240044
avg_rivfldsto	Time-mean river and floodplain storage	m^3	235414
darv	Depth-averaged river velocity	$m s^{-1}$	240045
avg_darv	Time-mean depth-averaged river velocity	$m s^{-1}$	235415
gwus	Groundwater storage	$kg m^{-2}$	240028

https://doi.org/10.5194/egusphere-2026-4305
Preprint. Discussion started: 4 September 2026
© Author(s) 2026. CC BY 4.0 License.

3.6 Operational monitoring and forecast setup

The IFS operational configuration for producing ensemble hydrological predictions (see Sect. 3.3.1) relies on a set of hydrological simulations (see Fig. 5) where the different modelling options are combined to generate climatological simulations, river thresholds and ensemble forecasts. The following simulations are part of the hydrological modelling workflow, and they were designed, tested and implemented as part of the integration of rivers in IFS.

IFS river reference: These are long global deterministic simulations using a 1-way coupling configuration (see Fig. 3c), with ERA5 meteorological forcings and the land surface version from the latest available IFS cycle (currently Cycle 49r1). Rivers and land are simulated at different spatial resolutions (i.e., TCo399, TCo1279 and TCo2559 for land; 15, 6, 3, and 1 arcmin for rivers), and output time steps range from hourly to daily. The river simulation is initialised from seasonal average state files (see Sect. 3.3.2 on initialisation) in 1979, and it continues until catching up with real time. After that, the simulation is updated daily, running only a few days behind real time. It provides a homogeneous representation of real-world rivers for climate monitoring, generates initial conditions for hydrological reforecasts and enables the computation of hydrological reference statistics (e.g., flood thresholds).

IFS river analysis: This is a deterministic global simulation using the operational configuration (see Fig. 3a), consisting of 2-way atmosphere-land coupling and a 1-way land-to-rivers coupling. The atmosphere and land components of the simulation are based on the IFS ensemble control member short forecast (i.e., the integration covering the interval between two consecutive forecasts) and the simulation is run for the most recent years. In the operational forecast system as of January 2026, the IFS river analysis provides river states at the start of each IFS forecast cycle at 3 arcmin spatial resolution and is executed twice daily, in line with the main IFS production cycles. The analysed river states are subsequently used as initial conditions for the operational hydrological ensemble forecasts. The IFS river analysis enables operational monitoring of river conditions that, in real time, are as close as possible to reality by leveraging the IFS data assimilation system, while for historical periods, it ensures full consistency with the operational forecasting configuration.

IFS real-time river ensemble forecast: This is a global ensemble simulation using the operational configuration (see Fig. 3a), consisting of 2-way atmosphere-land coupling and 1-way land-to-rivers coupling. The atmosphere and land components of the simulation are based on the IFS major forecast cycle, with all members initialised from the same river analysis. The IFS real-time river ensemble forecasts generate the evolution of river conditions into the future, with the same modelling configuration that can be used for forecasts of different ranges, from medium to seasonal.

As of January 2026, the IFS river analysis and the IFS real-time river ensemble forecasts (15 day forecast horizon) are produced operationally every 12 hours (base time of 00 and 12 UTC) at 3 arcmin spatial resolution and hourly time steps. The archival frequency of the river variables matches the frequency used for atmosphere and land variables. The forecast simulations are currently archived in MARS for internal use, with public release planned for the next scientific model upgrade.

https://doi.org/10.5194/egusphere-2026-4305
Preprint. Discussion started: 4 September 2026
© Author(s) 2026. CC BY 4.0 License.

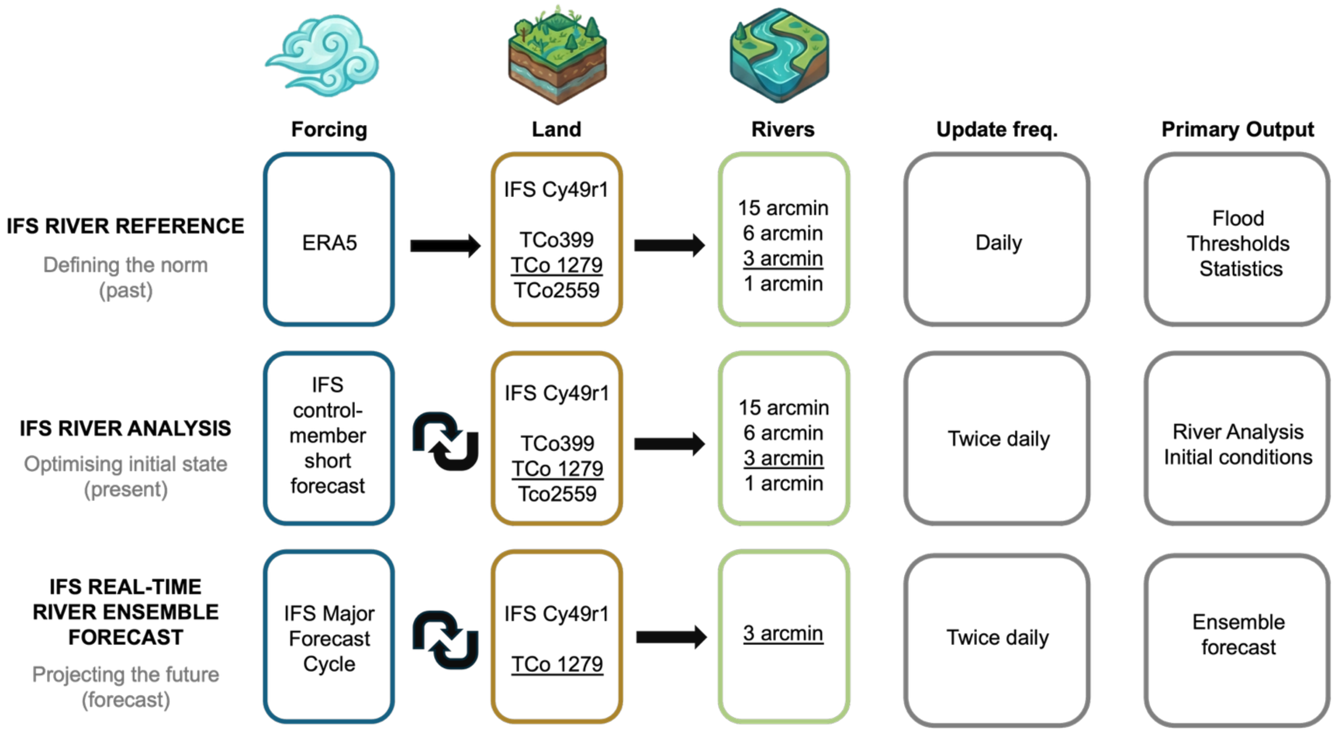

Figure 5: Schematic representation of the simulations that are part of the IFS hydrological modelling workflow. Underlined text identifies the spatial resolution used in the operational configuration as of January 2026.

4 Applications

The integration of river routing as an operational component of IFS enables ECMWF to produce daily and sub-daily global high-resolution river analyses, as well as real-time medium-range ensemble forecasts of river discharge and flood inundation, supporting disaster risk reduction and early warning systems at local, regional, and global scales with skilful hydrological forecasts with lead time compatible with anticipatory actions.

The system's capacity to generate multi-decadal river discharge datasets at daily and sub-daily timesteps provides a robust foundation for diverse hydrological applications, including assessment of extreme events (floods and droughts), long-term variability and trends in global water resources, and training datasets for machine learning hydrological models. Gridded river discharge, water level, and inundated areas are included as default diagnostic variables within the IFS hydrological modelling framework. To reduce computational costs, the land and river components can be executed over regional domains (using 1-way atmosphere-to-land-to-rivers coupling) at user-specified spatial resolutions, facilitating post-event analysis and model development activities.

The capability to perform kilometre-scale simulations, using temporal resolutions ranging from sub-daily (e.g., 1 hourly) to daily, is particularly valuable for early warning and preparedness applications, as fine spatial resolution reduces the risk of impact overestimation associated with partial flooding representation in coarser model grids. Accurate representation of

https://doi.org/10.5194/egusphere-2026-4305
Preprint. Discussion started: 4 September 2026
© Author(s) 2026. CC BY 4.0 License.

flood extent constitutes an important milestone for ECMWF's Earth system modelling approach, as inundated areas could in the future be incorporated into 2-way coupled simulations with re-evaporation and re-infiltration processes, enhancing the physical realism of flood impact representation.

This section presents applications that demonstrate the capabilities of different components and products of the operational hydrology system, with lead times sufficient for anticipatory action and decision-making. These applications illustrate three key capabilities enabled by the integration of CaMa-Flood within IFS: (i) operational forecasting of river discharge and flood area, (ii) high-resolution regional hydrological analysis, and (iii) diagnostic and cross-component evaluation of the land water cycle. An overview of the applications with details about the simulation setup, main products and scope is given in Table 2.

Table 2 List of applications where rivers are used in the ecLand and IFS simulations.

Application	Simulation type and configuration	Main product	Use
WMO State of Global Water Resources Report, 2024	IFS river reference Global 6 arcmin rivers Daily	Daily river discharge for the period 1991 2020 and 2024	Global water resources monitoring
Queensland floods, 2025	IFS river reference IFS river analysis IFS real-time river ensemble forecast Global 3 arcmin rivers 6 hourly	Flood thresholds Post-event analysis Step-by-step flood hydrographs	River flow forecasts for extreme events
Zambesi floods, 2023	1-way coupling experiment Regional Land and rivers at 1arcmin, 3arcmin, 6arcmin Daily	Daily river water level Flood inundated areas	Regional high-resolution simulations for flood risk assessment
Pakistan floods, 2022	IFS river analysis Global 3 arcmin rivers 6 hourly	Flood inundated areas	Assessment of flood inundation extent

https://doi.org/10.5194/egusphere-2026-4305
Preprint. Discussion started: 4 September 2026
© Author(s) 2026. CC BY 4.0 License.

ecLand wetland module development	IFS river reference	Flood inundated fraction	Improving Carbon fluxes representation

4.1 Global Water Resources monitoring with IFS rivers

The IFS river reference simulation (see Sect. 3.6), produced at 6 arcmin spatial resolution and daily output time steps, was ECMWF's dataset contribution to the WMO State of Global Water Resources Report (World Meteorological Organization, 2025), and it represents an example of the use of the IFS river reference simulation for monitoring rivers and floodplains globally. The report presents a quantitative assessment of global water resources for the year 2024, based on 12 simulated reference datasets (including IFS river reference) covering both the 1991-2020 reference period and 2024. It provides a global reference for river discharge, supporting the monitoring of climate variability and long-term trends. Model simulations also help compensate for spatial gaps and disparities in hydrometric observations worldwide. Findings from the State of Global Water Resources Report contribute to the WMO Early Warning for All initiative by serving as a scientific foundation for developing tools to manage water-related hazards (e.g., floods and droughts).

Figure 6 presents the annual mean river discharge for 2024, derived from the IFS river reference dataset, which was produced using a 1-way atmosphere-to-land-to-rivers modelling configuration, using ERA5 forcings, the land surface model from IFS Cycle 48r1 on the TCo1279 grid (i.e., ~9 km resolution) and rivers at 6 arcmin spatial resolution (i.e., ~11.1 km at the Equator).

https://doi.org/10.5194/egusphere-2026-4305
Preprint. Discussion started: 4 September 2026
© Author(s) 2026. CC BY 4.0 License.

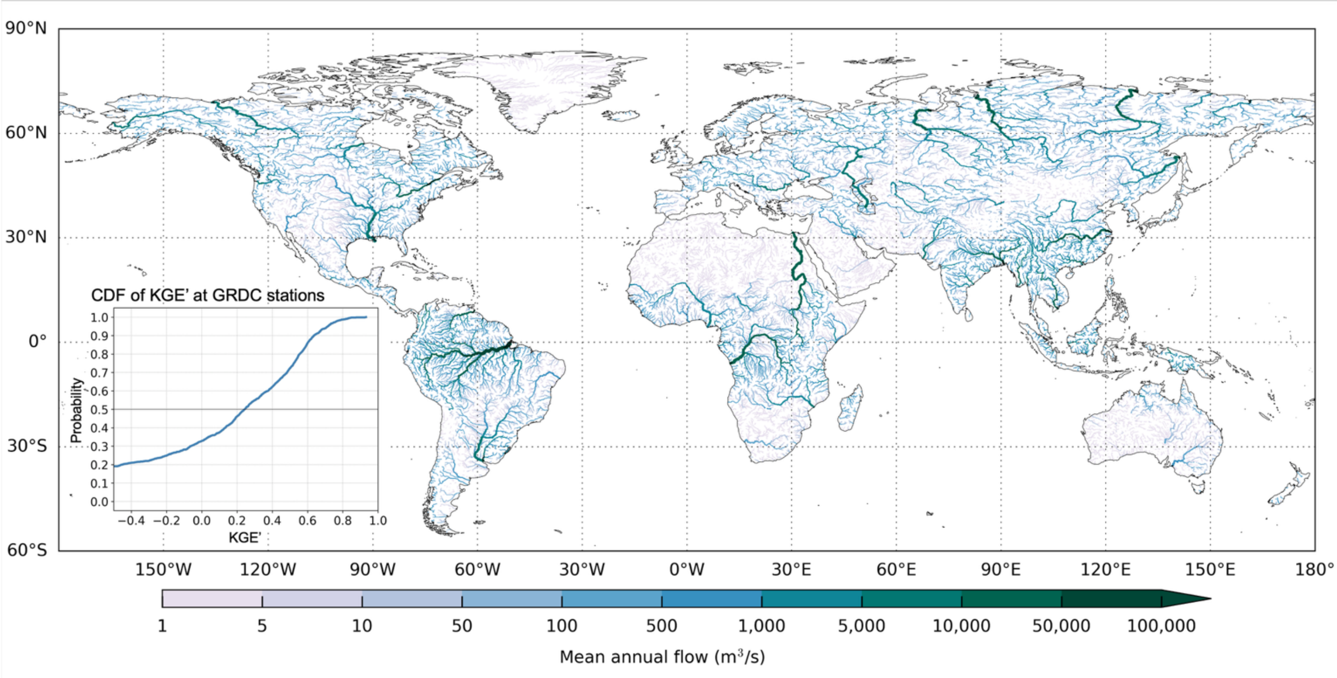

Figure 6: Annual mean river discharge for 2024 derived from the IFS river reference simulation with 1-way atmosphere-to-land-to-rivers coupling produced by ECMWF for the 2024 WMO State of Global Water Resources Report. The inset figure shows the hydrological skill calculated over the 1991-2020 period at about 1300 Global Runoff Data Centre (GRDC) stations globally, evaluated by the modified Kling-Gupta efficiency metric (Gupta et al., 2009; Kling et al., 2012) (ideal value is 1; skill threshold of -0.41).

4.2 River flow forecasts for extreme events: the Queensland floods, 2025

IFS river analysis and IFS real-time river ensemble forecasts can be used during flood events to generate analysis and forecast products. Figure 7 presents examples of hydrological products generated for the state of Queensland (northeastern Australia; dark grey area in Fig. 7a) covering the period from the end of January to early February 2025, when an active monsoon phase produced several tropical lows with a prolonged period of heavy rainfall. This resulted in major flooding in the Burdekin River (see https://www.bom.gov.au/qld/flood/brochures/burdekin/burdekin.shtml, last access: 24 March 2026), a 129,000 km^2 catchment and the largest river within the study area (highlighted by a red rectangle in Fig. 7a). The hydrological products were produced using the IFS river analysis for post-event summary assessment (see Fig. 7b and 7c) and the IFS real-time ensemble forecast for step-by-step river flow forecast visualisation (see Fig. 7d-f), both configured with rivers at 3 arcmin spatial resolution and 6 hourly output time steps. The IFS river reference simulation for the period 2005-2024 and a Gumbel distribution fitted on the river discharge annual maxima were used to define return periods for the Burdekin River catchment.

Between 31 January and 13 February 2025, the IFS river analysis simulated the river discharge to exceed the 20 year return period level (i.e., 5% annual exceedance probability) in the majority of the Burdekin River basin, with extreme floods (>50

https://doi.org/10.5194/egusphere-2026-4305
Preprint. Discussion started: 4 September 2026
© Author(s) 2026. CC BY 4.0 License.

year return period level, 2% annual exceedance probability) in large sections of the catchment (see Fig. 7b). In the whole study area, 13.1% of the river grid cells belong to the 'Extreme' category, meaning river flow exceeded the 50 year return period during the event.

The simulated flood wave in the IFS river analysis started on 1 February in the upstream part of the catchment, and then it moved downstream with the peak flow reaching the Sellheim River station (20.0064°S 146.4373°E) on 3 February (see Fig. 7c), when 26.9% of river grid cells observed the maximum river flow in the study area.

Seven days before the peak (forecast run of 29 January 00 UTC; Fig. 7d), the ensemble forecast generated by the IFS real-time river ensemble forecast showed a flood peak around 3 or 4 February at Sellheim station, with the 90th percentile reaching ~15,000 m^3/s (upper light blue shade) and large uncertainty in the magnitude and timing of the peak. Five days before the event, the uncertainty in the flood peak timing decreased, with the forecast flood magnitude rising to about 24,000 m^3/s (forecast run of 31 January 00 UTC; Fig. 7e). Three days before the event, the flood signal was strong, with the peak expected in the early hours on 3 February, matching the IFS river analysis very closely (forecast run of 2 February 00 UTC; Fig. 7f). Moreover, the river discharge observations (dashed black lines in Fig. 7d-f) highlight that the simulated flood wave was realistic both in magnitude and timing, although it showed a slight underestimation of the peak magnitude and an earlier than observed arrival time.

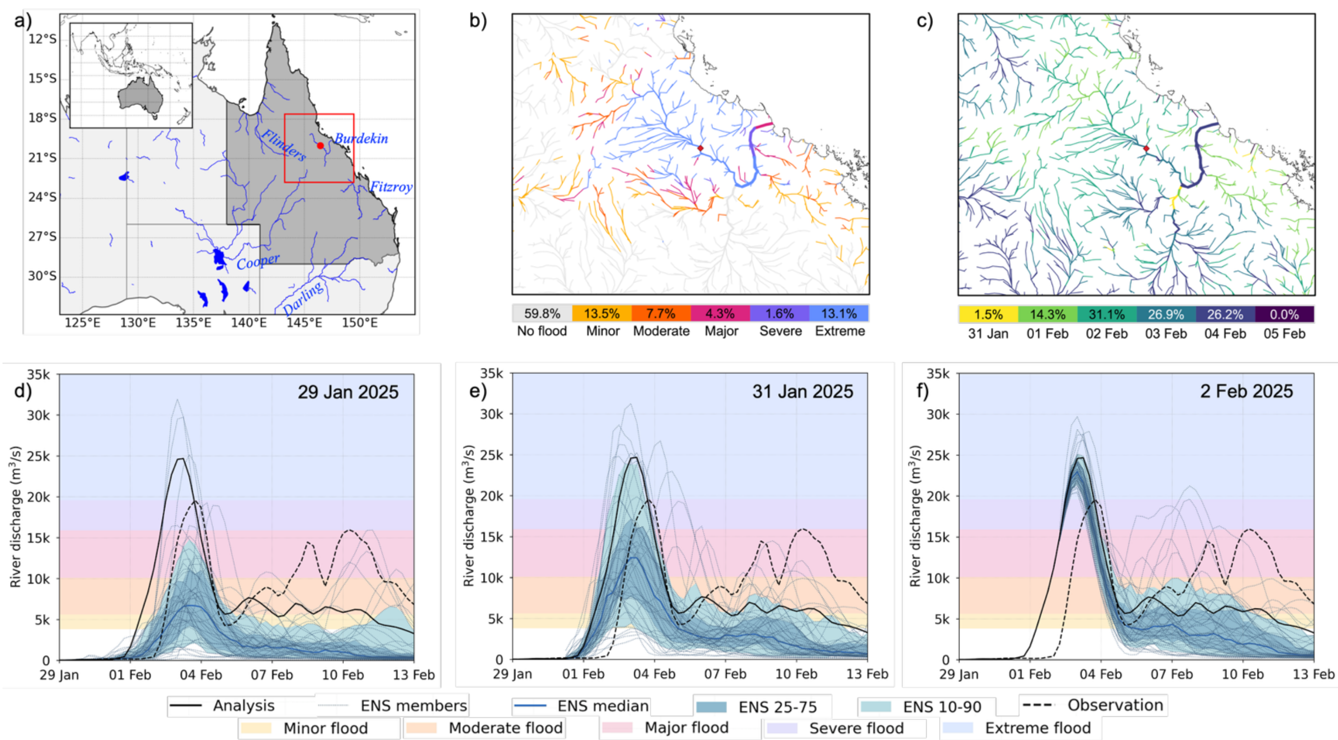

Figure 7: Example of IFS river analysis and real-time river ensemble discharge forecast for the Queensland floods (Australia) from late January to early February 2025. (a): Map of Australia showing the state of Queensland (dark grey) and major rivers (blue). The red marker indicates the Burdekin River at Sellheim, for which forecast hydrographs are presented in panels (d-f). The red rectangle denotes the study area shown in panels (b) and (c). (b): Maximum simulated flood severity from the IFS river

https://doi.org/10.5194/egusphere-2026-4305
Preprint. Discussion started: 4 September 2026
© Author(s) 2026. CC BY 4.0 License.

analysis (colours) over 31 January-5 February 2025. Numbers indicate the proportion of impacted river pixels within the study area. (c): Date of peak flood occurrence (in 00 UTC intervals) derived from the IFS river analysis for the same period, with numbers indicating the proportion of impacted river pixels. (d-f): Medium-range 6 hourly ensemble river discharge forecast initialised at 00 UTC on 29 January, 31 January and 2 February 2025 at Sellheim (location shown in panels a-c). The river analysis is shown in black, individual ensemble members in thin dark blue lines, the ensemble median in thick blue, and observations in dashed black. The 10th–90th percentile range is indicated by light blue shading, and the interquartile range by darker blue shading. Background colours represent flood severity categories. The flood severity in (b) is defined according to estimated flood return periods (RP): grey: no flood (RP ≤ 1.5 years); light orange: minor flood (1.5 < RP ≤ 2 years); orange: moderate flood (2 < RP ≤ 5 years); dark pink: major flood (5 < RP ≤ 20 years); purple: severe flood (20 < RP ≤ 50 years); sky blue: extreme flood (RP > 50 years). Return periods are estimated using a Gumbel distribution fitted to annual maximum discharge from the IFS river reference simulation for 2005–2024.

4.3 Regional high-resolution simulations for efficient flood risk assessment: the Zambezi floods, 2023

In 2023, the Zambezi River in Zambia experienced some of the worst floods in over 50 years, driven by weeks of heavy rainfall, leading to casualties, the displacement of several thousand households and the destruction of critical infrastructure (International Federation of Red Cross and Red Crescent Societies (IFRC), 2023). Three regional simulations for the period 2019 to 2023 were set up over the Luangwa River catchment, a tributary of the Zambezi River and one of the last free-flowing rivers in southern Africa that runs from northeastern Zambia, near Malawi, to the southwestern part of the country, to the border with Mozambique and Zimbabwe (see Fig. 8a). The three regional simulations were produced using a 1-way atmosphere-to-land-to-rivers modelling configuration (see Sect. 3.3.1), driven by ERA5 forcings, with both the regional version of ecLand from IFS Cycle 49r1 and the river model configured at 1, 3 and 6 arcmin spatial resolution, and outputs generated at daily time steps. The simulations show water on the Luangwa River in the Chipuka area (upstream drainage area of 41,000 km², red dot in Fig. 8a-b) matching both the timing and magnitude of observed water levels as derived from satellite altimetry measurements (Schwatke et al., 2015), in particular for the highest peak on 19 March 2023 (estimated at 557.96 m ± 0.15 m above mean sea level; see Fig. 8c). The simulated flooded fraction area on 19 March 2023 is shown for the three different spatial resolution experiments in Fig. 8d-f. As spatial resolution increases, the flooded area (calculated as the grid cell area multiplied by the flooded fraction) decreases (from 2,525 km^2 for 6 arcmin, 1,533 km^2 for 3 arcmin and down to 912 km^2 for 1 arcmin) as does uncertainty in the flood signal, with a higher proportion of the flooded grid cells simulated as completely underwater at 1 arcmin. (see Fig. 8g-i).

The ability to run kilometre-scale simulations is particularly valuable for early warning and preparedness, as it reduces impact overestimation associated with the exaggerated spatial extent of partial flooding in coarser-resolution model grids. In contrast, higher-resolution simulations exhibit a larger proportion of severely flooded pixels, indicating that coarser configurations tend to under-represent flood severity. An example is given for the estimation of the population, livestock and crops potentially affected by river flooding, based on the total exposure within areas where the estimated flooded fraction is greater than zero. The estimated exposed population decreases from over 7,000 in the 6 arcmin simulation to 6,000 and 3,500 in the 3 arcmin and 1 arcmin simulations, respectively. Similarly, livestock exposure ranges from approximately 85,000 to 28,900 animals for the 6 arcmin and 1 arcmin simulations. Higher-resolution simulations show a greater proportion of severely flooded pixels, indicating more intense local impacts. As a result, despite the lower overall exposure, the actual

https://doi.org/10.5194/egusphere-2026-4305
Preprint. Discussion started: 4 September 2026
© Author(s) 2026. CC BY 4.0 License.

risk, particularly for small livestock (e.g., poultry), may be higher at finer spatial resolutions. This highlights the strong sensitivity of both exposure and risk estimates to the spatial resolution of the river model.

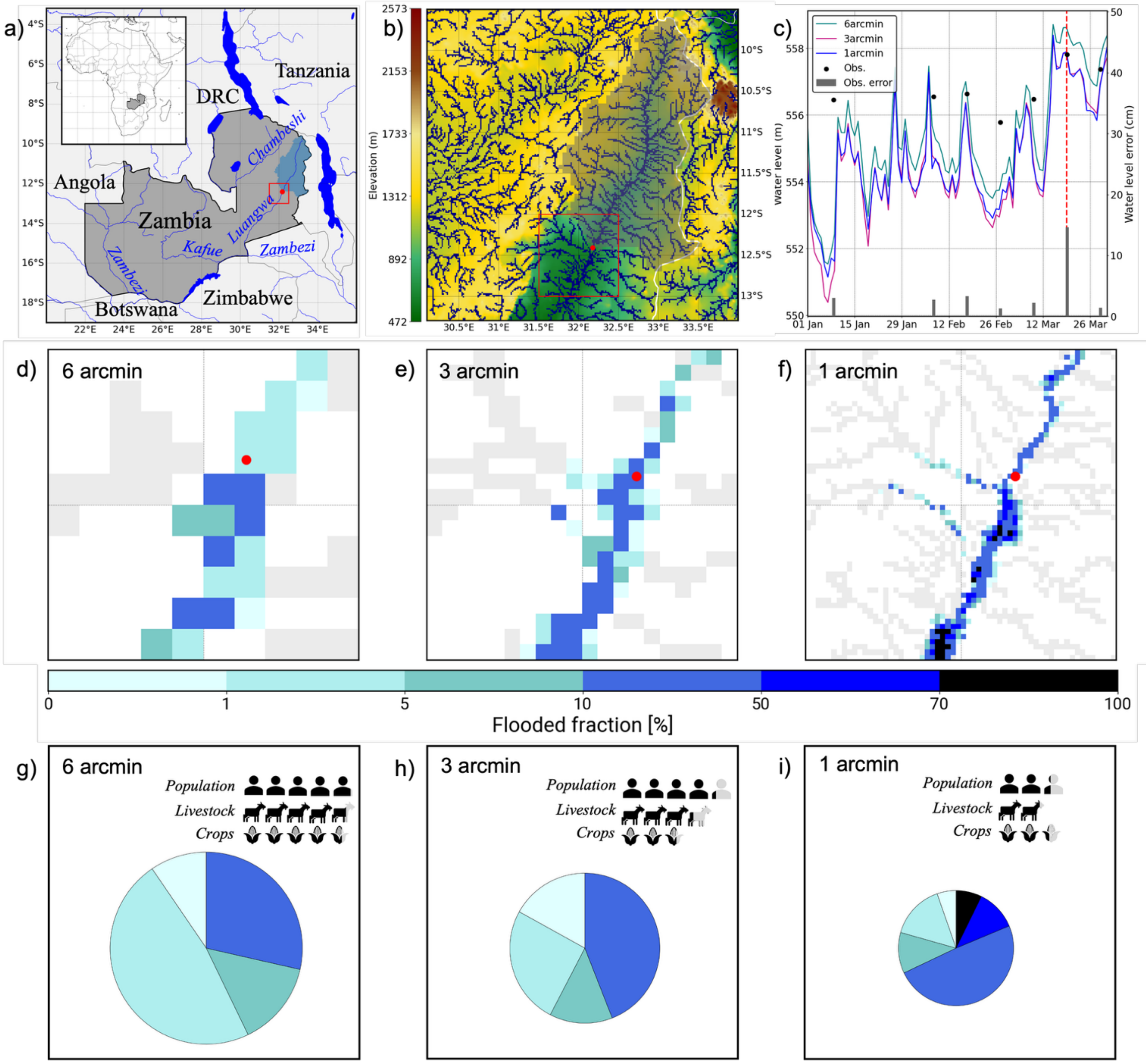

Figure 8: Results from the 1-way coupled regional simulations for the Luangwa River, Zambia. (a): Overview of the study region, with the study area indicated by a red rectangle and the evaluation point at Chipuka (red dot; 32.16ºE, -12.42ºS) along the Luangwa River. (b): Topography and 1 arcmin river network (blue), with the study area highlighted by the red rectangle. (c): Daily water level time series from 1 January to 31 March 2023, comparing 1-way coupled simulations (continuous lines) with satellite altimetry-derived observations (black dots; Schwatke et al., 2015) (d-f): Modelled flooded fraction on 19 March 2023 at 6, 3, and 1 arcmin spatial resolution, respectively. (g-i): Estimated flood impact metrics at the three spatial resolutions, showing flooded surface area (pie chart radius), proportion of flooded fraction (pie wedge area), and critical exposure within inundated

https://doi.org/10.5194/egusphere-2026-4305
Preprint. Discussion started: 4 September 2026
© Author(s) 2026. CC BY 4.0 License.

areas (defined as flooded fraction > 0) for residential population (icon = 1,500 persons), livestock (icon = 15,000 livestock), and crops (icon = 25 km²). Exposure datasets from WorldPop project (Bondarenko et al., 2025) at a 92.77m resolution from 2020 (population); AGLW (Du et al., 2025) at a 10 km nominal resolution from 2020 (livestock) and Copernicus Global Land Cover dataset version 3 2019, at a 100 m resolution (Copernicus Land Monitoring Service and Copernicus Land Monitoring Service Helpdesk, 2015) (cropland).

4.4 Representing flood inundation extent: Pakistan floods, 2022

Thanks to the flexibility of CaMa-Flood integration in IFS (see Sect. 3.3), land and river spatial resolutions are independent of the atmospheric grid in the operational configuration, and river simulations at a higher spatial resolution can be produced to improve hydrodynamic representation. An example is given for the floods over Pakistan (Arshad et al., 2025) on 27 August 2022 as observed by MODIS satellite (see Fig. 9b) and the flooded fraction simulated by the IFS river analysis at 3 arcmin (see Fig. 9c). This exceptional event was caused by a combination of high and persistent monsoon rainfall (for about 15 days) and enhanced glacier melt driven by a preceding heatwave, both of which are linked with climate change (Nanditha et al., 2023). The capacity of accurately representing the flood extent constitutes an important milestone for the Earth system approach embraced at ECMWF, since the inundated areas can be considered for re-evaporation and re-infiltration in a 2-way coupled system, enhancing the realism of the flooding impact.

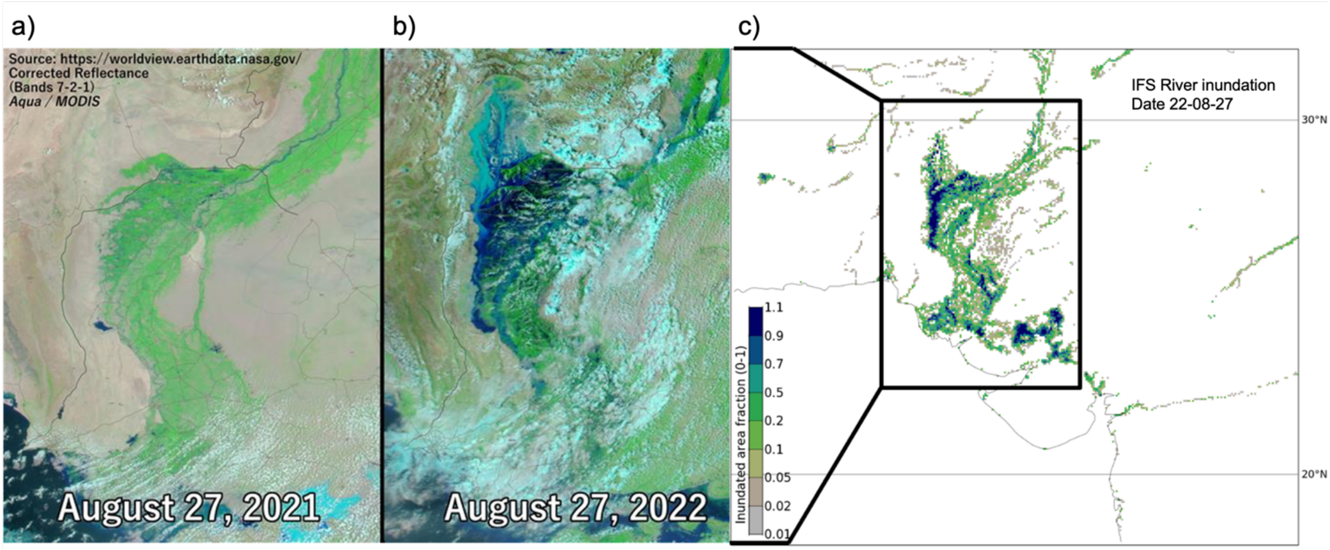

Figure 9: Inundation extent in Pakistan on 27 August 2022. Panel (a) shows MODIS-derived inundation for a reference year (2021), panel (b) presents MODIS observations for 27 August 2022 (both from NASA Worldview https:/worldview.earthdata.nasa.gov/) and panel (c) displays the corresponding IFS river analysis simulation at 3 arcmin spatial resolution.

4.5 Improving Carbon fluxes representation

Within the ecLand framework, a wetland CH_4 module has been developed to improve historical and forecast atmospheric concentrations of biogenic methane (CH_4) emissions in support of the ongoing improvements to the Copernicus Atmosphere

https://doi.org/10.5194/egusphere-2026-4305
Preprint. Discussion started: 4 September 2026
© Author(s) 2026. CC BY 4.0 License.

Monitoring Service (CAMS, https://atmosphere.copernicus.eu/, last access: 24 March 2026). The simple wetland parameterisation is based on previous models using temperature, wetland fraction and a representation of carbon availability for methanogenesis (Bloom et al., 2017). The simplicity of the parameterisation was chosen in response to previous work showing only minor impact on model performance with added complexity (McNorton et al., 2016). A Q_{10} function (temperature-dependent scaling factor) is applied to the uppermost soil temperature, T, taken from ecLand at computational timesteps (~5 minutes), as in (Gedney et al., 2004). As a proxy for substrate availability, the formulation of soil respiration for CO_2 from (Boussetta et al., 2013b) is used, which depends on a plant function type-dependent soil respiration, Re_0, and soil moisture and snow attenuation functions (f_{sm} and f_{sn}, respectively). The grid cell wetland fraction, f_{wet}, and a global or regional scaling factor, S, based on globally optimised surface fluxes (Saunois et al., 2020), are applied to obtain a surface CH_4 flux, F_{CH4}, as given by Eq. (1).

$$F_{CH_4} = S f_{wet} f_{sm} f_{sn} Re_0 Q_{10}^{\frac{T-25}{10}} \quad (1)$$

with $f_{sm} = \frac{\bar{\theta}}{\theta_{cap}}$ and $f_{sn} = 1 - C_{vs}(1 - e^{-\alpha z_{snow}})$,

where C_{vs} is the surface fraction covered by snow, a is a constant expressing the attenuation of the soil CO_2 emission within the snowpack, and z_{snow} is the snow depth, θ is soil moisture, and θ_{cap} is soil moisture at field capacity.

Since the operational configuration of Cycle 49r1, the IFS wetland component uses a monthly climatology based on the IFS river reference simulation and satellite data. Over all land points, the monthly total wetland fraction is first calculated as the sum (capped to 1) of the monthly flooded fraction of the IFS river reference simulation for the year 2019 and the monthly average from the Global Inundation Extent from Multi-Satellites (GIEMS) dataset (calculated over 1992-2020, v3.1; Prigent et al., 2007) after regridding to a common 0.1° resolution. Monthly IFS lake cover and agricultural inundated areas (defined according to a rice mask) are then removed with a minimum fraction set to 0. Finally, the resulting wetland map are converted into IFS climate fields for all relevant resolutions. Prior to its release, the impact of the CH_4 wetland model was tested using the CAMS CH_4 forecasting system (Agustí-Panareda et al., 2023) benchmarked against the Cycle 48r1 operational CAMS configuration. Whilst the Cycle 49r1 configuration represents a first use of the IFS river outputs operationally, work is underway to integrate both real-time satellite data, the IFS river analysis and IFS rivers forecasts within the operational workflow, to better represent both the interannual variability in wetland fraction and the forecast wetland emissions.

https://doi.org/10.5194/egusphere-2026-4305
Preprint. Discussion started: 4 September 2026
© Author(s) 2026. CC BY 4.0 License.

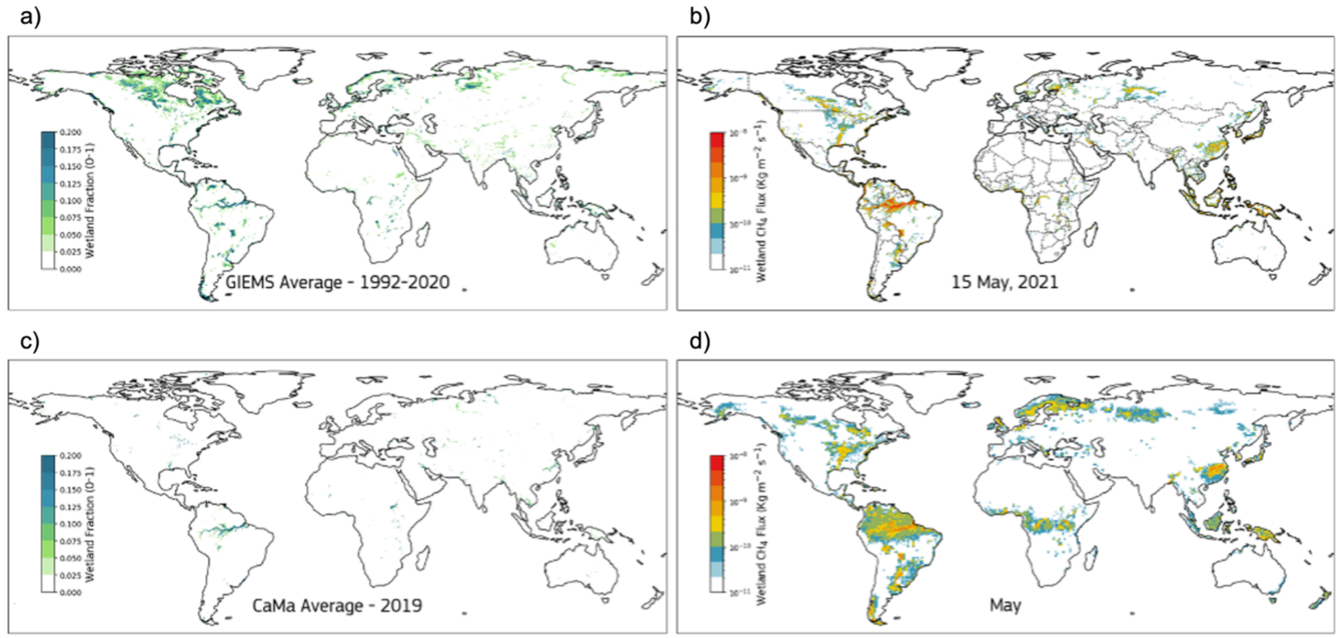

Figure 10: Global wetland inundation and associated methane (CH_4) fluxes. (a): Global average wetland inundation from satellite observations from 1992-2020 and (c): from IFS reference simulation (flood fraction) for 2019. (b): Wetland CH_4 flux from IFS output informed by both GIEMS and CaMa-Flood for 15 May 2021 and (d): the offline monthly climatology flux used since Cycle 49r1.

4.6 Land water as a diagnostic for the land water cycle

Thanks to the integrating properties of the water exchanges in space and time, river discharge is a useful tool to diagnose the land water cycle as simulated by Earth system models (Prudhomme et al., 2024). The inclusion of rivers in ECMWF's Earth system framework has enabled a fast, efficient, and systematic assessment of hydrological fluxes in any of its modelling chains, whether under research development for model evolution or in its operational context. This section presents several examples illustrating how river discharge has been used for land water budget diagnostics. The examples span different stages of maturity, from developments already implemented in operational IFS cycles to ongoing experimental investigations informed by the river routing scheme. An overview of these examples is provided in Table 3.

Table 3 Overview of examples illustrating the use of river discharge for land water budget diagnostics.

Diagnostic example	IFS component	Trigger	Stage
Evaluating snow–soil interactions in cold regions	Snow scheme	Representation of river discharge in permafrost areas	Contributed to developments released in IFS Cycle 49r1
Investigating persistent dry	Soil moisture DA	High river discharge levels triggered	Contributed to

https://doi.org/10.5194/egusphere-2026-4305
Preprint. Discussion started: 4 September 2026
© Author(s) 2026. CC BY 4.0 License.

bias in IFS over West Africa		by an excessive subsurface runoff generation mainly over the winter months	developments released in IFS Cycle 49r1
Investigating surface runoff generation at different spatial resolutions	Runoff generation	River discharge discrepancies in orographically complex areas between different spatial resolutions	Ongoing investigation
Coupling land surface runoff to ocean freshwater inputs	NEMO	Simulation of quantifiable and varying freshwater inputs into the ocean	Ongoing investigation

4.6.1 Evaluating snow–soil interactions in cold regions

Accounting for the influence of the cryosphere on surface temperature in high latitudes is a key component in ECMWF's Earth system approach. Following to the introduction of a new snow scheme (Arduini et al., 2019) in IFS Cycle 48r1, when the IFS ensemble medium-range modelling chain was upgraded to a ~9 km horizontal resolution, Zsoter et al. (2022) found an excessively rapid thawing of permafrost with the snow scheme of IFS Cycle 48r1, due to an overestimation of the heat transfer between the snowpack and the soil underneath, eventually leading to an excess of meltwater infiltrating into the soil rather than contributing to surface runoff. Several hydrological diagnostic experiments focusing on the representation of river discharge in permafrost areas (with 1-way atmosphere-to-land-to-rivers coupling) were conducted to identify the most appropriate parameterisation capable of improving the 2 temperature without deteriorating river behaviour, an integrated indicator of the land water budget. Using a sensitivity approach, a revised snow scheme was introduced in the IFS Cycle 49r1, showing improvement of river discharge simulation as well as snow depth and soil temperature (Cao et al., 2022).

4.6.2 Investigating persistent dry bias in IFS over West Africa

The difficulty in representing the West African monsoon system and its associated precipitation is a known issue in atmospheric science, both for climate monitoring and weather predictions (e.g., Kniffka et al., 2019; Lavers et al., 2022), leading to research into more complex moist physics (and subsequent operationalisation, e.g., in IFS Cycle 48r1; Bechtold et al., 2020) or into the use of data-driven techniques for improved parameterisation (e.g., Fischer et al., 2025). Whilst most of the studies have focused on atmosphere-only variables, a systematic assessment of the surface and subsurface runoff was conducted following the discovery of spurious flood peaks in West Africa outside the usual flood season in the operational IFS real-time river ensemble forecast. The hydrological diagnostic helped uncover the complex behaviour of a persistent dry bias in the atmosphere, present over the West African area, and its coupling with the soil moisture data assimilation algorithm. In the ECMWF's soil moisture assimilation system, the 2 m temperature and humidity are used as pseudo-observations of soil moisture to provide additional information to the analysis algorithm. Within this context, persistent negative temperature forecast anomalies indicated systematic positive soil moisture increments, attributed to the land data assimilation system trying to compensate for the dry humidity bias in the lowest part of the atmosphere through evaporation. The additional water added to the soil, locally reaching hundreds of mm mainly over the winter months, subsequently triggered excessive subsurface runoff generation in ecLand, leading to high river discharge levels. As a result of the investigations, a model extension to limit the adverse consequences of the dry bias was introduced in the IFS soil moisture data assimilation (included in the Cycle 49r1 model).

4.6.3 Investigating surface runoff generation at different spatial resolutions

The benefit of higher spatial resolution on the representation of the atmosphere and land processes has been investigated under the Destination Earth programme (DestinE; see https://destination-earth.eu/destination-earth/, last access: 25 March 2026). As part of the hydrological studies within DestinE, a 1-way land-to-river coupling experiment (~5.5 km river resolution) was performed using forcings from the Continuous Extremes Digital Twin (C-EDT; ~4.5 km, 2-way atmosphere–land coupling) and compared with the IFS river analysis at 6 arcmin (~9 km atmosphere–land, ~11 km river resolution) over the period 21 August 2023 to 31 January 2026. In orographically complex areas, C-EDT peak flows were systematically lower than those from the IFS river analysis, despite C-EDT precipitation totals being higher (Denissen et al., 2025). Further analyses of surface and subsurface runoff attributed the underestimation to the runoff generation scheme, where sub-grid orography influences the saturated fraction, which controls the saturation excess runoff processes.

The analysis of simulated river discharge time series in catchments located in orographically complex regions has triggered ongoing investigations into the parameterisation of key land-surface processes, with the aim of developing scale-adaptive formulations applicable across horizontal resolutions up to the kilometre scale.

4.6.4 Coupling land surface runoff to ocean freshwater inputs

As of IFS Cycle 49r1, the river discharge component of the ocean freshwater input for the IFS ocean model NEMO (Breivik et al., 2015) is provided by climatological values. The automatic simulation of river discharge within the IFS offers the opportunity to simulate quantifiable and varying freshwater inputs into the ocean when coupled with simulated river discharge, closing a vital link in the model's water cycle. As reported in previous studies (e.g., Zuo et al., 2020), updated freshwater inputs are expected to improve NEMO's freshwater plumes and make climatological runs more realistic in terms of freshwater input trends. The more integrated water cycle should ultimately lead to improved verification of the interconnected components (precipitation, soil moisture, runoff, river discharge, and ocean salinity). Development is ongoing to couple IFS river ocean outlet grid points to the nearest coastal grid point of NEMO's tripolar ORCA grid

https://doi.org/10.5194/egusphere-2026-4305
Preprint. Discussion started: 4 September 2026
© Author(s) 2026. CC BY 4.0 License.

5 Conclusions

The integration of the CaMa-Flood hydrodynamic model into the Integrated Forecast System marks a major milestone in ECMWF's Earth system modelling framework. The transition from an offline atmosphere-land-river configuration to an operational system that explicitly represents river routing and inundated areas enables ECMWF to routinely produce physically consistent, global, high-resolution river analyses and real-time ensemble forecasts. Hydrology is thus established as a standard component of the IFS, allowing the generation of river discharge, river water level, and flood inundation fields as gridded forecast products.

All river output variables have been assigned a GRIB2 parameter code and have been submitted and approved by the WMO, ensuring standardisation and long-term maintainability. The fields can now be archived directly to MARS, providing a single repository entry point for efficient retrieval by both internal and, in the future, external users.

The success of the integration of rivers in IFS relied heavily on software refactoring to ensure modularity and scalability. A key outcome of this effort is the maintenance of a single code base supporting operational, development, and diagnostics applications. Both ecLand and CaMa-Flood are fully open-source, ensuring transparency and reproducibility for the wider scientific community. The CaMa-Flood, ecLand, and IFS codes were refactored to provide a framework that is considerably more flexible, modular, and extensible than previous monolithic implementations. This refactoring also enables spatially distributed ecLand model parameters, replacing uniform values with two-dimensional fields.

The introduction of a hybrid MPI/OpenMP parallelisation for CaMa-Flood was essential to meet the high-resolution requirements (up to 3 arcmin or ~5km) of operational hydrological forecasting. Combined with the adoption of single-precision computation, this optimisation improved performance on high-performance computing architectures. It also prepares the system for future upgrades, including higher spatial and temporal resolutions (towards kilometric scale grids), larger ensemble sizes, extended lead times, and more frequent updates of the IFS river analysis and reference products.

The capability to run different modelling configurations enables a wide spectrum of applications, from operations to rapid diagnostic experiments to long-term research developments. By explicitly defining and labelling the simulations within the ensemble hydrological prediction system (e.g., IFS river reference, analysis, and ensemble forecast), the modelling workflow is structured consistently and transparently, thereby improving reproducibility and facilitating diagnostic evaluation.

Beyond its forecasting capability, rivers in IFS provide a powerful diagnostic tool for the entire land–water cycle. Because river discharge integrates water exchanges across space and time, it has been used to identify deficiencies within the IFS. For example, spurious flood peaks revealed a persistent dry bias in the West African monsoon linked to unintended interactions with soil moisture data assimilation. Hydrological diagnostics have also been used to refine snow–soil interaction parameterisations in cold regions, reducing the overestimation of permafrost thaw, and experiments conducted within the DestinE programme indicated the need for adaptive runoff parameterisations as model resolution approaches the kilometre scale.

The IFS river reference has already proven its value, serving as a contribution to the WMO State of Global Water Resources Report. This dataset provides a robust foundation for assessing climate variability and monitoring water-related hazards globally, especially in regions where in situ hydrometric observations are sparse.

The inclusion of rivers in IFS is designed for further evolution and opens multiple perspectives for monitoring, forecasting and benchmarking, linking more tightly land surface hydrological improvements with impact on the whole Earth system.

Looking ahead, the system evolution will focus on implementing and testing new processes impacting on the water-energy exchanges (including for example reservoirs or river levees), exploitation of the modular software and flexible data exchange capabilities (e.g., for parameters fine tuning, data assimilation, input to other components such as oceans, or development of a 2-way coupled system) or generation of physically-realistic global datasets of the hydrosphere to better leverage the power of AI in Earth system modelling.

Code and data availability

Model codes developed at ECMWF are the intellectual property of ECMWF and its member states, and therefore, the IFS code is not publicly available. ECMWF member-state weather services and their approved partners will get access granted. The OpenIFS code is available as open-source software under the Apache-2.0 license at https://github.com/ecmwf-ifs/openifs. More details can be found at https://confluence.ecmwf.int/display/OIFS/About+OpenIFS (ECMWF, 2026a) (last access: 28 March 2026). The ecLand code is available as open-source software on the ECMWF-IFS GitHub repository under the Apache-2.0 licence at https://github.com/ecmwf-ifs/ecland. The CaMa-Flood code is available as open-source software under the Apache-2.0 licence at https://github.com/global-hydrodynamics/CaMa-Flood_v4. CaMa-Flood version (v4.24) used for this study is archived at Zenodo at https://zenodo.org/records/17053436. (Dai Yamazaki et al., 2025).

Author contributions

CM, HC, and CP contributed to conceptualisation. CM, HC, and CP prepared the original draft. DY, GB, SB, JD, MW, GA, GD, JMN, AAP, MT, EZ, MC, and CR contributed to the drafting, reviewing, and editing of the manuscript. CM, GB, SB, MW, GD, JMN, AAP, MT, and EZ developed the visualisations. ED, and FP contributed to the review of the manuscript.

Competing interests

The authors declare that they have no conflict of interest.

https://doi.org/10.5194/egusphere-2026-4305
Preprint. Discussion started: 4 September 2026
© Author(s) 2026. CC BY 4.0 License.

Disclaimer

Copernicus Publications remains neutral with regard to jurisdictional claims made in the text, published maps, institutional affiliations, or any other geographical representation in this paper. While Copernicus Publications makes every effort to include appropriate place names, the final responsibility lies with the authors. Views expressed in the text are those of the authors and do not necessarily reflect the views of the publisher.

Acknowledgements

During the preparation of this work, the authors used AI-assisted tools (ChatGPT, OpenAI and NotebookLM, Google) to edit, shorten, and improve the readability of the manuscript. After using this tool/service, the authors reviewed and edited the content as needed and take full responsibility for the content of the publication. Parts of Figure 3 and part of Figure 5 were generated using AI-assisted tools (NotebookLM, Google) and subsequently modified by the authors. For Figure 9 we acknowledge the use of imagery from the NASA Worldview application (https://worldview.earthdata.nasa.gov), part of the NASA Earth Science Data and Information System (ESDIS). The work presented in Sect. 4.6.3 has been produced in the context of the European Union's Destination Earth Initiative and relates to tasks entrusted by the European Union to the European Centre for Medium-Range Weather Forecasts, implementing part of this initiative with funding by the European Union. The authors would like to thank Luis E. Samaniego and Stephan Thober from the Helmholtz Centre for Environmental Research (UFZ), and Etienne Tourigny and Iria Ayan from the Barcelona Supercomputing Centre (BSC), for their valuable contributions to the IFS development.

References

Agustí-Panareda, A., Barré, J., Massart, S., Inness, A., Aben, I., Ades, M., Baier, B. C., Balsamo, G., Borsdorff, T., Bousserez, N., Boussetta, S., Buchwitz, M., Cantarello, L., Crevoisier, C., Engelen, R., Eskes, H., Flemming, J., Garrigues, S., Hasekamp, O., Huijnen, V., Jones, L., Kipling, Z., Langerock, B., McNorton, J., Meilhac, N., Noël, S., Parrington, M., Peuch, V.-H., Ramonet, M., Razinger, M., Reuter, M., Ribas, R., Suttie, M., Sweeney, C., Tarniewicz, J., and Wu, L.: Technical note: The CAMS greenhouse gas reanalysis from 2003 to 2020, Atmos. Chem. Phys., 23, 3829–3859, https://doi.org/10.5194/acp-23-3829-2023, 2023.

Alfieri, L., Burek, P., Dutra, E., Krzeminski, B., Muraro, D., Thielen, J., and Pappenberger, F.: GloFAS – global ensemble streamflow forecasting and flood early warning, Hydrol. Earth Syst. Sci., 17, 1161–1175, https://doi.org/10.5194/hess-17-1161-2013, 2013.

Arduini, G., Balsamo, G., Dutra, E., Day, J. J., Sandu, I., Boussetta, S., and Haiden, T.: Impact of a Multi-Layer Snow Scheme on Near-Surface Weather Forecasts, J Adv Model Earth Syst, 11, 4687–4710, https://doi.org/10.1029/2019MS001725, 2019.

Arduini, G., Rüdiger, C., and Balsamo, G.: Enhancing the Representation of Glaciers and Ice Sheets in the ecLand Land-Surface Model: Impacts on Surface Energy Balance and Hydrology Across Scales, The Cryosphere, 20, 1119–1137, https://doi.org/10.5194/tc-20-1119-2026, 2026.

Arshad, A., Mirchi, A., He, C., Shah, A. A., and AghaKouchak, A.: Anthropogenic and climatic drivers of the 2022 mega-flood in Pakistan, npj Nat. Hazards, 2, 57, https://doi.org/10.1038/s44304-025-00109-z, 2025.

Baatz, R., Hendricks Franssen, H. J., Euskirchen, E., Sihi, D., Dietze, M., Ciavatta, S., Fennel, K., Beck, H., De Lannoy, G., Pauwels, V. R. N., Raiho, A., Montzka, C., Williams, M., Mishra, U., Poppe, C., Zacharias, S., Lausch, A., Samaniego, L., Van Looy, K., Bogena, H., Adamescu, M., Mirtl, M., Fox, A., Goergen, K., Naz, B. S., Zeng, Y., and Vereecken, H.: Reanalysis in Earth System Science: Toward Terrestrial Ecosystem Reanalysis, Reviews of Geophysics, 59, e2020RG000715, https://doi.org/10.1029/2020RG000715, 2021.

Bahra, A., Russell, I., and Kertész, S.: ecFlow 5 brings benefits to Member States, ECMWF Newsletter No 166, Winter 2020/21, 33–35, 2021.

Balsamo, G., Beljaars, A., Scipal, K., Viterbo, P., Van Den Hurk, B., Hirschi, M., and Betts, A. K.: A Revised Hydrology for the ECMWF Model: Verification from Field Site to Terrestrial Water Storage and Impact in the Integrated Forecast System, Journal of Hydrometeorology, 10, 623–643, https://doi.org/10.1175/2008JHM1068.1, 2009.

Balsamo, G., Salgado, R., Dutra, E., Boussetta, S., Stockdale, T., and Potes, M.: On the contribution of lakes in predicting near-surface temperature in a global weather forecasting model, Tellus A: Dynamic Meteorology and Oceanography, 64, 15829, https://doi.org/10.3402/tellusa.v64i0.15829, 2012.

Balsamo, G., Mogensen, K., Keeley, S., Bidlot, J.-R., Boussetta, S., Dutra, E., and Wedi, N.: Coupling of oceans and land surfaces in the ECMWF Integrated Forecasting System: Sensitivity and impact of diurnal and synoptic variability on medium-range skill, WGNE Blue Book 2017, 2017.

Bechtold, P., Forbes, R., Sandu, I., Lang, S., and Ahlgrimm, M.: A major moist physics upgrade for the IFS, ECMWF Newsletter No 164, Summer 2020, 24–32, https://doi.org/10.21957/3GT59VX1PB, 2020.

Bidlot, J.-R. and Janssen, P.: Ocean–wave-related changes in the next model upgrade, ECMWF Newsletter No 179, Spring 2024, 18–25, 2024.

Bloom, A. A., Bowman, K. W., Lee, M., Turner, A. J., Schroeder, R., Worden, J. R., Weidner, R., McDonald, K. C., and Jacob, D. J.: A global wetland methane emissions and uncertainty dataset for atmospheric chemical transport models (WetCHARTs version 1.0), Geosci. Model Dev., 10, 2141–2156, https://doi.org/10.5194/gmd-10-2141-2017, 2017.

Bondarenko, M., Priyatikanto, R., Tejedor Garavito, N., Zhang, W., McKeen, T., Cunningham, A., Woods, T., Hilton, J., Cihan, D., Nosatiuk, B., Brinkhoff, T., Tatem, A., and Sorichetta, A.: Constrained estimates of 2015-2030 total number of people per grid square at a resolution of 3 arc (approximately 100m at the equator) R2025A version v1., https://doi.org/10.5258/SOTON/WP00839, 2025.

https://doi.org/10.5194/egusphere-2026-4305
Preprint. Discussion started: 4 September 2026
© Author(s) 2026. CC BY 4.0 License.

Boussetta, S., Balsamo, G., Beljaars, A., Kral, T., and Jarlan, L.: Impact of a satellite-derived leaf area index monthly climatology in a global numerical weather prediction model, International Journal of Remote Sensing, 34, 3520–3542, https://doi.org/10.1080/01431161.2012.716543, 2013a.

Boussetta, S., Balsamo, G., Beljaars, A., Panareda, A., Calvet, J., Jacobs, C., Van Den Hurk, B., Viterbo, P., Lafont, S., Dutra, E., Jarlan, L., Balzarolo, M., Papale, D., and Van Der Werf, G.: Natural land carbon dioxide exchanges in the ECMWF integrated forecasting system: Implementation and offline validation, JGR Atmospheres, 118, 5923–5946, https://doi.org/10.1002/jgrd.50488, 2013b.

Boussetta, S., Balsamo, G., Arduini, G., Dutra, E., McNorton, J., Choulga, M., Agustí-Panareda, A., Beljaars, A., Wedi, N., Munõz-Sabater, J., De Rosnay, P., Sandu, I., Hadade, I., Carver, G., Mazzetti, C., Prudhomme, C., Yamazaki, D., and Zsoter, E.: ECLand: The ECMWF Land Surface Modelling System, Atmosphere, 12, 723, https://doi.org/10.3390/atmos12060723, 2021.

Breivik, Ø., Mogensen, K., Bidlot, J., Balmaseda, M. A., and Janssen, P. A. E. M.: Surface wave effects in the NEMO ocean model: Forced and coupled experiments, JGR Oceans, 120, 2973–2992, https://doi.org/10.1002/2014JC010565, 2015.

Buizza, R., Andersson, E., Forbes, R., and Sleigh, M.: The ECMWF research to operations (R20) process, Technical Memorandum, https://doi.org/10.21957/M3R9BVG6X, 2017.

Buizza, R., Alonso Balmaseda, M., Brown, A., English, S. J., Forbes, R., Geer, A., Haiden, T., Leutbecher, M., Magnusson, L., Rodwell, M., Sleigh, M., Stockdale, T., Vitart, F., and Wedi, N.: The development and evaluation process followed at ECMWF to upgrade the Integrated Forecasting System (IFS), Technical Memorandum, https://doi.org/10.21957/XZOPNHTY9, 2018.

Burton, P., Battino, P., Sleigh, M., and Sahin, C.: Building NEXhub: an infrastructure for the future of IFS experimentation, ECMWF Newsletter No 185, Autumn 2025, https://doi.org/10.21957/HWDC-8W27, 2025.

Bush, M., Boutle, I., Edwards, J., Finnenkoetter, A., Franklin, C., Hanley, K., Jayakumar, A., Lewis, H., Lock, A., Mittermaier, M., Mohandas, S., North, R., Porson, A., Roux, B., Webster, S., and Weeks, M.: The second Met Office Unified Model–JULES Regional Atmosphere and Land configuration, RAL2, Geosci. Model Dev., 16, 1713–1734, https://doi.org/10.5194/gmd-16-1713-2023, 2023.

Cao, B., Arduini, G., and Zsoter, E.: Brief communication: Improving ERA5-Land soil temperature in permafrost regions using an optimized multi-layer snow scheme, The Cryosphere, 16, 2701–2708, https://doi.org/10.5194/tc-16-2701-2022, 2022.

Carver, G.: Ten years of OpenIFS at ECMWF, ECMWF Newsletter No 170, Winter 2021/22, 6–7, 2022.

Copernicus Land Monitoring Service and Copernicus Land Monitoring Service Helpdesk: Land Cover 2015-2019 (raster 100 m), global, annual - version 3 (3.0), https://doi.org/10.2909/C6377C6E-76CC-4D03-8330-628A03693042, 2015.

Dai Yamazaki, Menaka Revel, Misako Hatono, Michel Wortmann, Risa Hanazaki, Tomoko Nitta, Xudong Zhou, Shengyu Kang, DirkEilander, and Fang Zhao: global-hydrodynamics/CaMa-Flood_v4: v4.24, , https://doi.org/10.5281/ZENODO.17053436, 2025.

De Rosnay, P., Browne, P., De Boisséson, E., Fairbairn, D., Hirahara, Y., Ochi, K., Schepers, D., Weston, P., Zuo, H., Alonso-Balmaseda, M., Balsamo, G., Bonavita, M., Borman, N., Brown, A., Chrust, M., Dahoui, M., Chiara, G., English, S., Geer, A., Healy, S., Hersbach, H., Laloyaux, P., Magnusson, L., Massart, S., McNally, A., Pappenberger, F., and Rabier, F.: Coupled data assimilation at ECMWF: current status, challenges and future developments, Quart J Royal Meteoro Soc, 148, 2672–2702, https://doi.org/10.1002/qj.4330, 2022.

Denissen, J., Arduini, G., Zsoter, E., Wortmann, M., Tanguy, M., Gascón, E., Mazzetti, C., Prudhomme, C., Morrison, O., Düben, P., Sandu, I., Rüdiger, C., and Vannière, B.: The role of sub-grid orography for global high-resolution flood forecasting, European Geosciences Union General Assembly 2025 (EGU25), held 27 April-2 May, 2025 in Vienna, Austria. Online at https://www.egu25.eu/, id. EGU25-7097, https://doi.org/10.5194/egusphere-egu25-7097, 2025.

Dorigo, W., Himmelbauer, I., Aberer, D., Schremmer, L., Petrakovic, I., Zappa, L., Preimesberger, W., Xaver, A., Annor, F., Ardö, J., Baldocchi, D., Bitelli, M., Blöschl, G., Bogena, H., Brocca, L., Calvet, J.-C., Camarero, J. J., Capello, G., Choi, M., Cosh, M. C., Van De Giesen, N., Hajdu, I., Ikonen, J., Jensen, K. H., Kanniah, K. D., De Kat, I., Kirchengast, G., Kumar Rai, P., Kyrouac, J., Larson, K., Liu, S., Loew, A., Moghaddam, M., Martínez Fernández, J., Mattar Bader, C., Morbidelli, R., Musial, J. P., Osenga, E., Palecki, M. A., Pellarin, T., Petropoulos, G. P., Pfeil, I., Powers, J., Robock, A., Rüdiger, C., Rummel, U., Strobel, M., Su, Z., Sullivan, R., Tagesson, T., Varlagin, A., Vreugdenhil, M., Walker, J., Wen, J., Wenger, F., Wigneron, J. P., Woods, M., Yang, K., Zeng, Y., Zhang, X., Zreda, M., Dietrich, S., Gruber, A., Van Oevelen, P., Wagner, W., Scipal, K., Drusch, M., and Sabia, R.: The International Soil Moisture Network: serving Earth system science for over a decade, Hydrol. Earth Syst. Sci., 25, 5749–5804, https://doi.org/10.5194/hess-25-5749-2021, 2021.

Du, Z., Yu, L., Zhao, Y., Li, X., Liu, X., Li, X., Hao, P., Chen, Z., Guo, Z., You, L., Ma, X., and Wang, H.: Annual global grided livestock mapping from 1961 to 2021, Earth Syst. Sci. Data, 17, 5543–5556, https://doi.org/10.5194/essd-17-5543-2025, 2025.

Dutra, E., Balsamo, G., Viterbo, P., Miranda, P. M. A., Beljaars, A., Schär, C., and Elder, K.: An Improved Snow Scheme for the ECMWF Land Surface Model: Description and Offline Validation, Journal of Hydrometeorology, 11, 899–916, https://doi.org/10.1175/2010JHM1249.1, 2010.

ECMWF: ECMWF Strategy 2021-2030, ECMWF, https://doi.org/10.21957/s21ec694kd, 2021.

ECMWF: IFS Documentation CY49R1 - Part II: Data Assimilation, ECMWF, https://doi.org/10.21957/105CB1333C, 2024a.

ECMWF: IFS Documentation CY49R1 - Part IV: Physical Processes, ECMWF, https://doi.org/10.21957/C731EE1102, 2024b.

ECMWF: IFS Documentation CY49R1 - Part VI: Technical and Computational Procedures, ECMWF, https://doi.org/10.21957/D52E494677, 2024c.

ECMWF: IFS Documentation CY49R1 (Parts I-VII), ECMWF, 2024d.

ECMWF: ECMWF Strategy 2025-2034, ECMWF, https://doi.org/10.21957/05dd9b657e, 2025.

ECMWF: About OpenIFS, 2026a.

ECMWF: Building a data-driven Earth system model at ECMWF, Destination Earth, 2026b.

Emerton, R., Zsoter, E., Arnal, L., Cloke, H. L., Muraro, D., Prudhomme, C., Stephens, E. M., Salamon, P., and Pappenberger, F.: Developing a global operational seasonal hydro-meteorological forecasting system: GloFAS-Seasonal v1.0, Geosci. Model Dev., 11, 3327–3346, https://doi.org/10.5194/gmd-11-3327-2018, 2018.

Emerton, R. E., Stephens, E. M., Pappenberger, F., Pagano, T. C., Weerts, A. H., Wood, A. W., Salamon, P., Brown, J. D., Hjerdt, N., Donnelly, C., Baugh, C. A., and Cloke, H. L.: Continental and global scale flood forecasting systems, WIREs Water, 3, 391–418, https://doi.org/10.1002/wat2.1137, 2016.

Fairbairn, D., De Rosnay, P., and Browne, P. A.: The New Stand-Alone Surface Analysis at ECMWF: Implications for Land–Atmosphere DA Coupling, Journal of Hydrometeorology, 20, 2023–2042, https://doi.org/10.1175/JHM-D-19-0074.1, 2019.

Fischer, M., Knippertz, P., and Proppe, C.: Surrogate-based model parameter optimization in simulations of the West African monsoon, Weather Clim. Dynam., 6, 113–130, https://doi.org/10.5194/wcd-6-113-2025, 2025.

Gedney, N., Cox, P. M., and Huntingford, C.: Climate feedback from wetland methane emissions, Geophysical Research Letters, 31, 2004GL020919, https://doi.org/10.1029/2004GL020919, 2004.

Gupta, H. V., Kling, H., Yilmaz, K. K., and Martinez, G. F.: Decomposition of the mean squared error and NSE performance criteria: Implications for improving hydrological modelling, Journal of Hydrology, 377, 80–91, https://doi.org/10.1016/j.jhydrol.2009.08.003, 2009.

Hanazaki, R., Yamazaki, D., and Yoshimura, K.: Development of a Reservoir Flood Control Scheme for Global Flood Models, J Adv Model Earth Syst, 14, e2021MS002944, https://doi.org/10.1029/2021MS002944, 2022.

Harrigan, S., Zsoter, E., Alfieri, L., Prudhomme, C., Salamon, P., Wetterhall, F., Barnard, C., Cloke, H., and Pappenberger, F.: GloFAS-ERA5 operational global river discharge reanalysis 1979–present, Earth Syst. Sci. Data, 12, 2043–2060, https://doi.org/10.5194/essd-12-2043-2020, 2020.

Harrigan, S., Cloke, H., and Pappenberger, F.: Innovating global hydrological prediction through an Earth system approach, WMO Bulletin, 69, 2023.

Herbert, C., De Rosnay, P., Weston, P., and Fairbairn, D.: Towards unified land data assimilation at ECMWF: Soil and snow temperature analysis in the SEKF, Quart J Royal Meteoro Soc, 150, 4133–4155, https://doi.org/10.1002/qj.4808, 2024.

Hirabayashi, Y., Tanoue, M., Sasaki, O., Zhou, X., and Yamazaki, D.: Global exposure to flooding from the new CMIP6 climate model projections, Sci Rep, 11, 3740, https://doi.org/10.1038/s41598-021-83279-w, 2021.

International Federation of Red Cross and Red Crescent Societies (IFRC): Zambia Flood in Southern Province, IFRC, 2023.

Isaksen, L., Bonavita, M., Buizza, R., Fisher, M., Haseler, J., Leutbecher, M., and Raynaud, L.: Ensemble of data assimilations at ECMWF, Technical Memorandum No 636, https://doi.org/10.21957/OBKE4K60, 2010.

Jonkman, S. N., Curran, A., and Bouwer, L. M.: Floods have become less deadly: an analysis of global flood fatalities 1975–2022, Nat Hazards, 120, 6327–6342, https://doi.org/10.1007/s11069-024-06444-0, 2024.

https://doi.org/10.5194/egusphere-2026-4305
Preprint. Discussion started: 4 September 2026
© Author(s) 2026. CC BY 4.0 License.

Kling, H., Fuchs, M., and Paulin, M.: Runoff conditions in the upper Danube basin under an ensemble of climate change scenarios, Journal of Hydrology, 424–425, 264–277, https://doi.org/10.1016/j.jhydrol.2012.01.011, 2012.

Kniffka, A., Knippertz, P., and Fink, A. H.: The role of low-level clouds in the West African monsoon system, Atmos. Chem. Phys., 19, 1623–1647, https://doi.org/10.5194/acp-19-1623-2019, 2019.

Kousal, J., Pelletier, C., Denissen, J. M. C., Schulte, L., Keeley, S., Dueben, P., Penny, S. G., Park, R.-S., Miralles, D. G., Shapkalijevski, M. M., Valmassoi, A., Renfrew, I., Zampieri, L., Kumar, R., Ruiz-Vásquez, M., Schulz, J.-P., Wu, L., and Pedruzo Bagazgoitia, X.: Numerical Weather Prediction Model Coupling—Strategies, Challenges, and Outlook, Bulletin of the American Meteorological Society, 107, E183–E189, https://doi.org/10.1175/BAMS-D-25-0270.1, 2026.

Lang, S., Alexe, M., Chantry, M., Dramsch, J., Pinault, F., Raoult, B., Clare, M. C. A., Lessig, C., Maier-Gerber, M., Magnusson, L., Bouallègue, Z. B., Nemesio, A. P., Dueben, P. D., Brown, A., Pappenberger, F., and Rabier, F.: AIFS -- ECMWF's data-driven forecasting system, https://doi.org/10.48550/ARXIV.2406.01465, 2024.

Lang, S., Alexe, M., Clare, M. C. A., Roberts, C., Adewoyin, R., Ben Bouallègue, Z., Chantry, M., Dramsch, J., Dueben, P. D., Hahner, S., Maciel, P., Prieto-Nemesio, A., O'Brien, C., Pinault, F., Polster, J., Raoult, B., Tietsche, S., and Leutbecher, M.: AIFS-CRPS: ensemble forecasting using a model trained with a loss function based on the continuous ranked probability score, npj Artif. Intell., 2, 18, https://doi.org/10.1038/s44387-026-00073-7, 2026.

Lang, S. T. K., Lock, S., Leutbecher, M., Bechtold, P., and Forbes, R. M.: Revision of the Stochastically Perturbed Parametrisations model uncertainty scheme in the Integrated Forecasting System, Quart J Royal Meteoro Soc, 147, 1364–1381, https://doi.org/10.1002/qj.3978, 2021.

Lavers, D. A., Simmons, A., Vamborg, F., and Rodwell, M. J.: An evaluation of ERA5 precipitation for climate monitoring, Quart J Royal Meteoro Soc, 148, 3152–3165, https://doi.org/10.1002/qj.4351, 2022.

Ma, W., Ishitsuka, Y., Takeshima, A., Hibino, K., Yamazaki, D., Yamamoto, K., Kachi, M., Oki, R., Oki, T., and Yoshimura, K.: Applicability of a nationwide flood forecasting system for Typhoon Hagibis 2019, Sci Rep, 11, 10213, https://doi.org/10.1038/s41598-021-89522-8, 2021.

Malardel, S., Wedi, N., Deconinck, W., Diamantakis, M., Kuehnlein, C., Mozdzynski, G., Hamrud, M., and Smolarkiewicz, P.: A new grid for the IFS, ECMWF Newsletter No 146, Winter 2015/16, 23–28, 2016.

McNorton, J., Gloor, E., Wilson, C., Hayman, G. D., Gedney, N., Comyn-Platt, E., Marthews, T., Parker, R. J., Boesch, H., and Chipperfield, M. P.: Role of regional wetland emissions in atmospheric methane variability, Geophysical Research Letters, 43, https://doi.org/10.1002/2016GL070649, 2016.

McNorton, J. R., Arduini, G., Bousserez, N., Agustí-Panareda, A., Balsamo, G., Boussetta, S., Choulga, M., Hadade, I., and Hogan, R. J.: An Urban Scheme for the ECMWF Integrated Forecasting System: Single-Column and Global Offline Application, J Adv Model Earth Syst, 13, e2020MS002375, https://doi.org/10.1029/2020MS002375, 2021.

Mizukami, N., Clark, M. P., Gharari, S., Kluzek, E., Pan, M., Lin, P., Beck, H. E., and Yamazaki, D.: A Vector-Based River Routing Model for Earth System Models: Parallelization and Global Applications, J Adv Model Earth Syst, 13, e2020MS002434, https://doi.org/10.1029/2020MS002434, 2021.

https://doi.org/10.5194/egusphere-2026-4305
Preprint. Discussion started: 4 September 2026
© Author(s) 2026. CC BY 4.0 License.

Moldovan, G., Pinnington, E., Prieto Nemesio, A., Lang, S., Ben Bouallègue, Z., Dramsch, J., Alexe, M., Santa Cruz, M., Hahner, S., Cook, H., Theissen, H., Clare, M., O'Brien, C., Polster, J., Magnusson, L., Mertes, G., Pinault, F., Raoult, B., De Rosnay, P., Forbes, R., and Chantry, M.: AIFS 1.1.0: An update to ECMWF's machine-learned weather forecast model AIFS, https://doi.org/10.5194/egusphere-2025-4716, 17 October 2025.

Muñoz-Sabater, J., Dutra, E., Agustí-Panareda, A., Albergel, C., Arduini, G., Balsamo, G., Boussetta, S., Choulga, M., Harrigan, S., Hersbach, H., Martens, B., Miralles, D. G., Piles, M., Rodríguez-Fernández, N. J., Zsoter, E., Buontempo, C., and Thépaut, J.-N.: ERA5-Land: a state-of-the-art global reanalysis dataset for land applications, Earth Syst. Sci. Data, 13, 4349–4383, https://doi.org/10.5194/essd-13-4349-2021, 2021.

Nanditha, J. S., Kushwaha, A. P., Singh, R., Malik, I., Solanki, H., Chuphal, D. S., Dangar, S., Mahto, S. S., Vegad, U., and Mishra, V.: The Pakistan Flood of August 2022: Causes and Implications, Earth's Future, 11, e2022EF003230, https://doi.org/10.1029/2022EF003230, 2023.

Nitta, T., Arakawa, T., Hatono, M., Takeshima, A., and Yoshimura, K.: Development of Integrated Land Simulator, Prog Earth Planet Sci, 7, 68, https://doi.org/10.1186/s40645-020-00383-7, 2020.

Pappenberger, F., Cloke, H. L., Balsamo, G., Ngo-Duc, T., and Oki, T.: Global runoff routing with the hydrological component of the ECMWF NWP system, Intl Journal of Climatology, 30, 2155–2174, https://doi.org/10.1002/joc.2028, 2010.

Pastorello, G., Trotta, C., Canfora, E., Chu, H., Christianson, D., Cheah, Y.-W., Poindexter, C., Chen, J., Elbashandy, A., Humphrey, M., Isaac, P., Polidori, D., Reichstein, M., Ribeca, A., Van Ingen, C., Vuichard, N., Zhang, L., Amiro, B., Ammann, C., Arain, M. A., Ardö, J., Arkebauer, T., Arndt, S. K., Arriga, N., Aubinet, M., Aurela, M., Baldocchi, D., Barr, A., Beamesderfer, E., Marchesini, L. B., Bergeron, O., Beringer, J., Bernhofer, C., Berveiller, D., Billesbach, D., Black, T. A., Blanken, P. D., Bohrer, G., Boike, J., Bolstad, P. V., Bonal, D., Bonnefond, J.-M., Bowling, D. R., Bracho, R., Brodeur, J., Brümmer, C., Buchmann, N., Burban, B., Burns, S. P., Buysse, P., Cale, P., Cavagna, M., Cellier, P., Chen, S., Chini, I., Christensen, T. R., Cleverly, J., Collalti, A., Consalvo, C., Cook, B. D., Cook, D., Coursolle, C., Cremonese, E., Curtis, P. S., D'Andrea, E., Da Rocha, H., Dai, X., Davis, K. J., Cinti, B. D., Grandcourt, A. D., Ligne, A. D., De Oliveira, R. C., Delpierre, N., Desai, A. R., Di Bella, C. M., Tommasi, P. D., Dolman, H., Domingo, F., Dong, G., Dore, S., Duce, P., Dufrêne, E., Dunn, A., Dušek, J., Eamus, D., Eichelmann, U., ElKhidir, H. A. M., Eugster, W., Ewenz, C. M., Ewers, B., Famulari, D., Fares, S., Feigenwinter, I., Feitz, A., Fensholt, R., Filippa, G., Fischer, M., Frank, J., Galvagno, M., et al.: The FLUXNET2015 dataset and the ONEFlux processing pipeline for eddy covariance data, Sci Data, 7, 225, https://doi.org/10.1038/s41597-020-0534-3, 2020.

Prigent, C., Papa, F., Aires, F., Rossow, W. B., and Matthews, E.: Global inundation dynamics inferred from multiple satellite observations, 1993–2000, J. Geophys. Res., 112, 2006JD007847, https://doi.org/10.1029/2006JD007847, 2007.

Prudhomme, C., Zsótér, E., Matthews, G., Melet, A., Grimaldi, S., Zuo, H., Hansford, E., Harrigan, S., Mazzetti, C., De Boisseson, E., Salamon, P., and Garric, G.: Global hydrological reanalyses: The value of river discharge information for

© Author(s) 2026. CC BY 4.0 License.

world-wide downstream applications – The example of the Global Flood Awareness System GloFAS, Meteorological Applications, 31, e2192, https://doi.org/10.1002/met.2192, 2024.

Roberts, C. D., Senan, R., Molteni, F., Boussetta, S., Mayer, M., and Keeley, S. P. E.: Climate model configurations of the ECMWF Integrated Forecasting System (ECMWF-IFS cycle 43r1) for HighResMIP, Geosci. Model Dev., 11, 3681–3712, https://doi.org/10.5194/gmd-11-3681-2018, 2018.

Santos, M. J., Medvigy, D., Silva Dias, M. A. F., Freitas, E. D., and Kim, H.: Seasonal Flooding Causes Intensification of the River Breeze in the Central Amazon, JGR Atmospheres, 124, 5178–5197, https://doi.org/10.1029/2018JD029439, 2019.

Sármány, D., Mogensen, K., Mirco Valentini, Razvan Aguridan, Philipp Geier, James Hawkes, Simon Smart, and Tiago Quintino: New software libraries for ORAS6 ocean reanalysis, ECMWF Newsletter No 178, Winter 2024, 13–15, 2024.

Saunois, M., Stavert, A. R., Poulter, B., Bousquet, P., Canadell, J. G., Jackson, R. B., Raymond, P. A., Dlugokencky, E. J., Houweling, S., Patra, P. K., Ciais, P., Arora, V. K., Bastviken, D., Bergamaschi, P., Blake, D. R., Brailsford, G., Bruhwiler, L., Carlson, K. M., Carrol, M., Castaldi, S., Chandra, N., Crevoisier, C., Crill, P. M., Covey, K., Curry, C. L., Etiope, G., Frankenberg, C., Gedney, N., Hegglin, M. I., Höglund-Isaksson, L., Hugelius, G., Ishizawa, M., Ito, A., Janssens-Maenhout, G., Jensen, K. M., Joos, F., Kleinen, T., Krummel, P. B., Langenfelds, R. L., Laruelle, G. G., Liu, L., Machida, T., Maksyutov, S., McDonald, K. C., McNorton, J., Miller, P. A., Melton, J. R., Morino, I., Müller, J., Murguia-Flores, F., Naik, V., Niwa, Y., Noce, S., O'Doherty, S., Parker, R. J., Peng, C., Peng, S., Peters, G. P., Prigent, C., Prinn, R., Ramonet, M., Regnier, P., Riley, W. J., Rosentreter, J. A., Segers, A., Simpson, I. J., Shi, H., Smith, S. J., Steele, L. P., Thornton, B. F., Tian, H., Tohjima, Y., Tubiello, F. N., Tsuruta, A., Viovy, N., Voulgarakis, A., Weber, T. S., Van Weele, M., Van Der Werf, G. R., Weiss, R. F., Worthy, D., Wunch, D., Yin, Y., Yoshida, Y., Zhang, W., Zhang, Z., Zhao, Y., Zheng, B., Zhu, Q., Zhu, Q., and Zhuang, Q.: The Global Methane Budget 2000–2017, Earth Syst. Sci. Data, 12, 1561–1623, https://doi.org/10.5194/essd-12-1561-2020, 2020.

Schwatke, C., Dettmering, D., Bosch, W., and Seitz, F.: DAHITI – an innovative approach for estimating water level time series over inland waters using multi-mission satellite altimetry, Hydrol. Earth Syst. Sci., 19, 4345–4364, https://doi.org/10.5194/hess-19-4345-2015, 2015.

Sleigh, M., Bennett, A., Burton, P., Cresswell, P., Gillies, P., Hill, A., Kipling, Z., Lange, M., Marsden, O., Nawab, A., and Reuter, B.: Modernisation of the Integrated Forecasting System, ECMWF Newsletter No 182, Winter 2024/25, 19–23, https://doi.org/10.21957/M9AD5HV72S, 2025.

Wedi, N. P., Hamrud, M., and Mozdzynski, G.: A Fast Spherical Harmonics Transform for Global NWP and Climate Models, Monthly Weather Review, 141, 3450–3461, https://doi.org/10.1175/MWR-D-13-00016.1, 2013.

Wedi, N. P., Polichtchouk, I., Dueben, P., Anantharaj, V. G., Bauer, P., Boussetta, S., Browne, P., Deconinck, W., Gaudin, W., Hadade, I., Hatfield, S., Iffrig, O., Lopez, P., Maciel, P., Mueller, A., Saarinen, S., Sandu, I., Quintino, T., and Vitart, F.: A Baseline for Global Weather and Climate Simulations at 1 km Resolution, J Adv Model Earth Syst, 12, e2020MS002192, https://doi.org/10.1029/2020MS002192, 2020.

https://doi.org/10.5194/egusphere-2026-4305
Preprint. Discussion started: 4 September 2026
© Author(s) 2026. CC BY 4.0 License.

Woldemeskel, F., Rüdiger, C., Yamazaki, D., Tian, S., Zhang, H., Marthews, T., Hou, J., Sharples, W., Su, C., Best, M., and Carrara, E.: Assessment of JULES Land Surface Model Coupled With CaMa -Flood for an Operational Streamflow Forecasting Across Australia, Hydrological Processes, 39, e70345, https://doi.org/10.1002/hyp.70345, 2025.

World Meteorological Organization: Congress endorses shift to Earth system approach, World Meteorological Organization (WMO), 2019.

World Meteorological Organization: WMO and the Early Warnings for All initiative, World Meteorological Organization (WMO), 2022.

World Meteorological Organization: State of Global Water Resources 2024, World Meteorological Organization, https://doi.org/10.59327/WMO/WATER/2024, 2025.

World Meteorological Organization (WMO): Vision and Strategy for Hydrology and Associated Plan of Action and WMO Hydrological Research Strategy, 2023 edition., World Meteorological Organization (WMO), Geneva, 57 pp., 2023.

Yamazaki, D.: Advancing global river hydrodynamics simulations by catchment-based macro-scale floodplain modeling approach, Geosci. Lett., 12, 72, https://doi.org/10.1186/s40562-025-00452-z, 2025.

Yamazaki, D., Kanae, S., Kim, H., and Oki, T.: A physically based description of floodplain inundation dynamics in a global river routing model, Water Resources Research, 47, 2010WR009726, https://doi.org/10.1029/2010WR009726, 2011.

Yamazaki, D., De Almeida, G. A. M., and Bates, P. D.: Improving computational efficiency in global river models by implementing the local inertial flow equation and a vector-based river network map, Water Resources Research, 49, 7221–7235, https://doi.org/10.1002/wrcr.20552, 2013.

Yamazaki, D., Ikeshima, D., Sosa, J., Bates, P. D., Allen, G. H., and Pavelsky, T. M.: MERIT Hydro: A High-Resolution Global Hydrography Map Based on Latest Topography Dataset, Water Resources Research, 55, 5053–5073, https://doi.org/10.1029/2019WR024873, 2019.

Zhao, G., Yamazaki, D., Tanaka, Y., Zhou, X., Li, S., Hu, Y., Hirabayashi, Y., Neal, J., and Bates, P.: Developing a Levee Module for Global Flood Modeling With a Reach-Level Parameterization Approach, Water Resources Research, 61, e2024WR039790, https://doi.org/10.1029/2024WR039790, 2025.

Zhu, Y., Fu, B., Yang, B., Guan, H., Sinsky, E., Li, W., Peng, J., Xue, X., Hou, D., Liang, X., and Shin, S.: Quantify the Coupled GEFS Forecast Uncertainty for the Weather and Subseasonal Prediction, JGR Atmospheres, 128, e2022JD037757, https://doi.org/10.1029/2022JD037757, 2023.

Zsoter, E., Arduini, G., Prudhomme, C., Stephens, E., and Cloke, H.: Hydrological Impact of the New ECMWF Multi-Layer Snow Scheme, Atmosphere, 13, 727, https://doi.org/10.3390/atmos13050727, 2022.

Zuo, H., De Boisseson, E., Zsoter, E., Harrigan, S., De Rosnay, P., Wetterhall, F., and Prudhomme, C.: Benefits of dynamically modelled river discharge input for ocean and coupled system., , https://doi.org/10.5194/egusphere-egu2020-8564, 2020.